Measurements of $\delta^{15}N$ and $\delta 40Ar$ of NEEM air with oxygen removal from a perovskite membrane

Alexander Erik Friisnæs
Master's Thesis
August 31th, 2021

Supervised by
Thomas Blunier
Professor
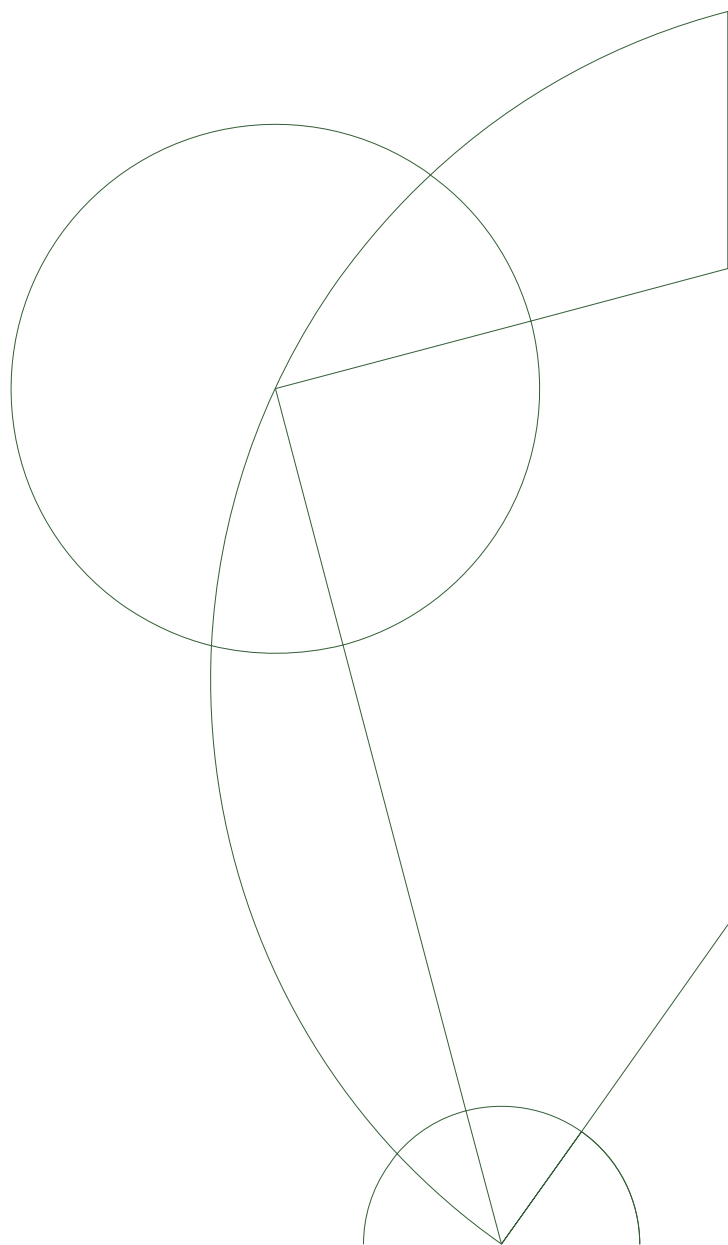
Abstract

Isotopes of nitrogen and argon are stable in the atmosphere over long periods of time but the isotopic abundances is subject to change in a firn column. Measurements of $\delta^{15}N$ and $\delta^{40}Ar$ from ice cores contains information about climate parameters such as temperature change through the firn and firn column width. With this information the past site temperature firn column height can be modelled. In this thesis a measurement system was built that could measure $\delta^{15}N$ and $\delta^{40}Ar$ as well as the zero-enrichment, pressure imbalance and chemical slope needed to analyze the δ values. A new oven was built to remove oxygen from the sample stream. The oven was found to have an oxygen removal rate of 99.4%. Four acquisition runs were carried out to test the stability of the setup. $\delta^{15}N$ was found to be: 4.787 ± 0.0120‰, 4.785 ± 0.0060‰, 4.649 ± 0.0070‰ and 4.503 ± 0.0689‰. The $\delta^{40}N$‰ was found to be: 6.078 ± 0.1581‰, 6.064 ± 0.0991‰, 5.8465 ± 0.0722‰ and 5.8519 ± 0.3687‰.

Acknowledgments

Contents

List of Figures

List of Tables

Chapter 1

Introduction

Current climate change is a well known and discussed topic in the global politics. The ramifications of climate change can be great and have devastating influence on populations all over the globe. Understanding the drivers and mechanism related to climate change of the past can increase the understanding of how the climate will change in the future [1]. When snow falls on ice sheets it slowly changes into firn and ice as the gravity and mass of fresh snow accumulates on top. In the firn layer atmospheric air can diffuse through the pores. When the firn transforms to ice, the atmospheric air in the firn will be trapped in gas bubbles [2]. The ice from the large continental ice sheets can be several hundred thousands years old and the gas trapped in the ice contains paleoclimatic information of the atmosphere at the time when the gas was trapped [3]. The isotopic compositions of nitrogen and argon are constant in the atmosphere over time scales of 10^5 years [4]. The isotopic abundances are changed by processes in polar firn. These processes are dependent on temperature and snow accumulation. Because of this the isotopic composition of stable isotopes of nitrogen and argon extracted from gas trapped in ice cores can be used to constrain the site temperature and accumulation rates. Measured isotopes can also be used to correct other elemental or isotopic quantities for the fractionation process in the firn column. Episodes of rapid climate change in the past, Dansgaard-Oeschger events, will therefor influence the isotopic compositions [5]. To sum up the measurements of $\delta^{15}N$ and $\delta^{40}Ar$ can be used as proxies to the temperature gradient in the firn and thickness of the diffusive firn column, and can be used to model the site temperature and firn height of the ice core location.[6]

1.1   Overview of this thesis

The goal of this thesis was to improve upon the existing gas line in view of the upcoming continues flow analysis (CFA) campaign to measure the Holocene section of the newly drilled EGRIP ice core. The old setup was taken apart after the last measurement campaign, the work in this thesis reflects the experimental challenges of building a new oven for oxygen removal (necessary for d15N and d40Ar measurements) and rebuilding the setup to measure $\delta^{15}N$ and $\delta^{40}Ar$ from sample air collected at the NEEM ice core

location.

Chapter 2 includes a theoretical introduction to the measurement of isotopes and δ values, a description of firn and fractionation processes, an introduction to mass spectrometry and Isodat, a description of the corrections applied to the measurements, a description and motivation for the removed gases and a description of the experimental setup.

Chapter 3 presents the results obtained while designing the oven, the signal intensities and isotopic and elemental ratios measured in this thesis, together with data for certain analytical test and corrects, namely, the zero enrichment measurement, the pressure imbalance measurement, the chemical slope measurement, the oxygen removal efficiency and the final measurements,final measurements, as raw data and values corrected for instrumental artifacts.

Chapter 4 is a discussion of the results presented in chapter 3 and a discussion of complications throughout the experimental work.

Chapter 5 includes the conclusion and an outlook for future optimization of the setup.

Chapter 2

Theoretical background and method

2.1 Stable Isotopes

An element always has the same number of protons in its nuclei, but the number of neutrons can vary. Elements with the same number of neutrons and a different number of protons are called isotopes. The atomic mass of an element is given by the sum of protons and neutrons. Isotopes have a different number of neutrons in their nuclei, the atomic mass of different isotopes of the same element is different. Different isotopes have different physical and chemical behavior. Radioactive isotopes are unstable and go through spontaneous decay; on the other hand, stable isotopes do not naturally decay. Stable isotopes are what this thesis will be concerned with. Table 2.1 shows the global averaged values of isotopic abundances of nitrogen, oxygen and argon.

Element	Isotope	Natural abundance
Nitrogen	14	99.63 %
Nitrogen	15	0.37 %
Oxygen	16	99.76 %
Oxygen	17	0.038 %
Oxygen	18	0.205 %
Argon	36	0.33 %
Argon	38	0.06 %
Argon	40	99.6 %

Table 2.1: table of the isotope abundances for N, O and Ar [7].

.

The standard notation of isotopes is as follows:

$$^{Z+N}_{Z}X^{N} \tag{2.1}$$

X denotes the element. Z denotes the number of protons. N denotes the number of neutrons. The form ^{Z+N}X is used in this thesis. The abundance of the argon isotope with

mass 40 is denoted ^{40}Ar. The sample isotopic abundances are compared with reference isotopic abundance measured from atmospheric air. There are two normal conventions that describe the ratios. The first is the ratio of the heavy to the light isotope. The second is the ratio of the rare and the common isotope. This thesis focuses on the stable isotopes ^{40}Ar and ^{15}N and uses the first convention. The abundance of stable isotopes in nature can vary depending on, in what reservoir they are located. There are some processes that can change the abundance of isotopes. These processes are called fractionation processes. Since stable isotopes can conserve climatic information, they are of great value to paleoclimatic research. Processes affecting nitrogen and argon stable isotopes will be explained in section 2.5.

An isotopic ratio is calculated as that of equation 2.2 where the concentration of the heavy isotope is in the numerator, and the concentration of the light isotope is in the denominator [8][9].

$$^{i}R = \frac{^{i}X}{^{j}X} \tag{2.2}$$

2.2 Delta notation

Being able to compare measurements of isotopic ratios to each other is of great importance. Therefore, isotopic ratios are commonly presented relative to a chosen reference. This is calculated with the δ notation, since the variation in the δ values are small, they are presented in per mil $[10^{-3}]$ or per meg $[10^{-6}]$. The δ value is of interest to research because it can be used as a proxy for climatic parameters. For measuring air compounds such as argon or nitrogen stable isotopes (R_{sample}), researchers present their data relative to the composition of recent atmospheric air ($R_{reference}$).

The delta notation is as follows:

$$\delta X = \left(\frac{R_{sample} - R_{reference}}{R_{reference}} \right) = \left(\frac{R_{sample}}{R_{reference}} - 1 \right) \tag{2.3}$$

δX is the relative difference between the ratio of a reference and sample gas.

The fractionation factor α is the ratio between R_{sample} and $R_{reference}$ and is defined as:

$$\alpha_{\frac{A}{B}} = \frac{R_A}{R_B} \tag{2.4}$$

where A denotes the sample and B denotes the reference. The fractionation factor describes when the isotopic ratio is changed through fractionation processes, either through chemical or physical processes [9] [8]. The fractionation effect is defined as:

$$\epsilon = \alpha - 1 \tag{2.5}$$

2.3 Firn processes

The firn column of an ice sheet is the uppermost layer and is 50-100 m deep [2]. Here the snow has yet to go through the transition to ice through densification. The transition hap-

pens through several different stages. When the precipitation falls as snow, the crystals are partially destroyed due to the wind, and the first layer is created. The snow is further compacted through the column by sublimation and re-sublimation. Then, part of crystals grow into a spherical shape at the cost of other crystals diminishing in size. At a depth of approximately 10 m and a density of approximately 550 $\frac{kg}{m^3}$, no more compaction can take place. The ice crystals are now packed closer due to ice sintering through pressure. Sintering is the process of decreasing the surface area of a porous solid at temperatures near the melting point[10].

At a density of approximately 810-840 $\frac{kg}{m^3}$, the ice crystals cannot be packed any closer, and no further diffusion of air can happen. The atmospheric air is now trapped as gas bubbles in the ice[2]. The densification profile is dependent on the temperature and accumulation and is different for each ice core. For the NEEM borehole, the close off depth was found at 78 m [11]. An illustrative sketch of a firn column can be seen in figure 2.1. The firn column has open pores, which means that air can diffuse through the firn. Throughout the densification process, the pores become smaller with depth until they are disconnected, and the channels are sealed off from the atmosphere.

Because the air in the open pores can still mix with the atmosphere, the age of the ice is older than the age of the air. The amount of annual precipitation and the site temperature affect the age difference.

Due to different dominating factors in gas transport, the firn column is divided into 3 different zones as seen in figure 2.1. The First zone is the convective zone where the gas can still exchange and mix freely with the atmosphere above through wind pumping [12], here δ is equivalent to the atmospheric values. Next, we have the diffusive zone where the gas moves primarily through molecular diffusion [13]. It is here that fractionation of the atmospheric air primarily happens. The two components that increase the signal of the δ values in the diffusive zone are gravitational fractionation and thermal fractionation. Due to gravity, heavier elements and isotopes are enriched at the bottom of the firn. Thermal fractionation is driven by temperature gradients through the firn column. This will cause the air to unmix, and the heavier isotopes will move towards the colder region and the lighter will move towards the warmer region. [9]. The final zone is the non-diffusive zone. In this zone, the gas is cut off from the diffusive zone. [14][15].
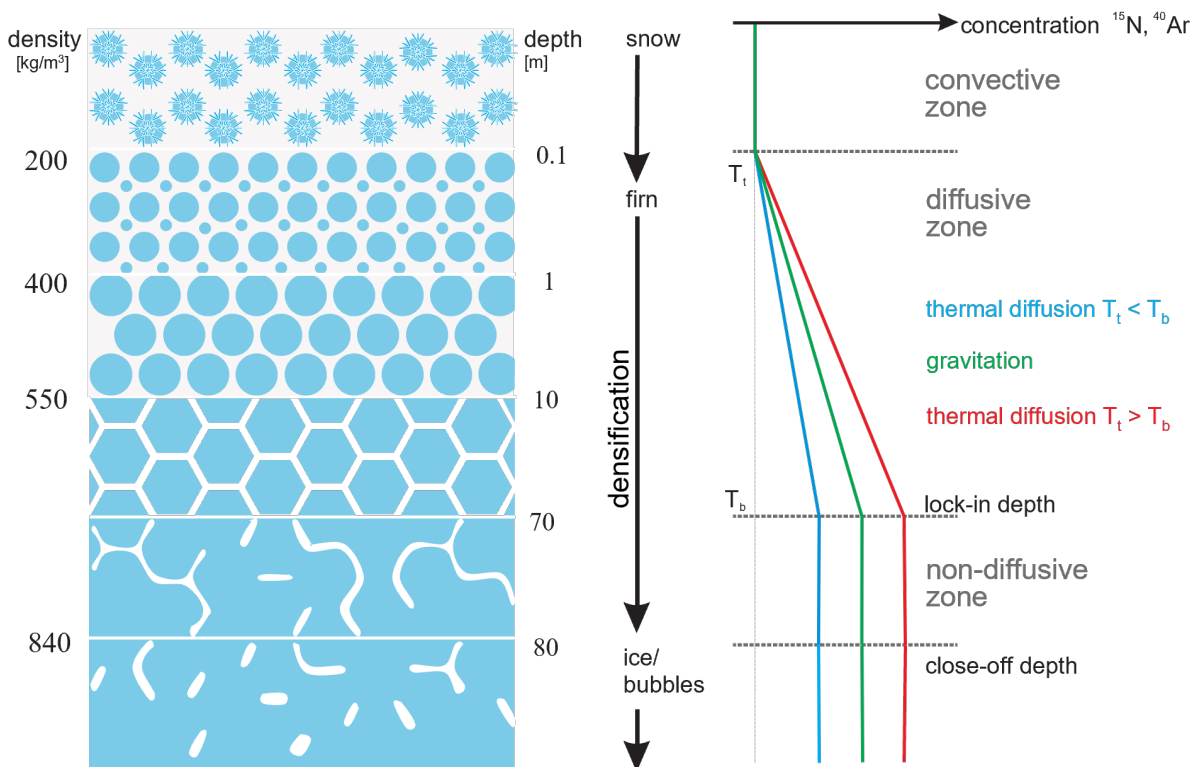
Figure 2.1: On the left, a sketch of a firn column and how the porosity and density change with depth. On the right, the $\delta^{15}N$ and $\delta^{40}Ar$ profiles are visualized. The green color shows the increase of $\delta^{15}N$ and $\delta^{40}Ar$ due to gravitational settling. The red and the blue line show the thermal diffusion effect on $\delta^{15}N$ and $\delta^{40}Ar$. The blue line describes the case of fast cooling at the surface where $\delta^{15}N$ and $\delta^{40}Ar$ decrease because the bottom of the firn is warmer than the top of the firn. The red line describes the case of fast warming at the surface where $\delta^{15}N$ and $\delta^{40}Ar$ increase because the bottom of the firn is colder than the top of the firn. Figure adapted from [2].

2.4   Relevance of Nitrogen and Argon

In this thesis, the focus is on nitrogen and argon stable isotopes. As shown in table 2.2, nitrogen is the most abundant gas, and argon is the third most abundant gas in the atmosphere. The isotopic compositions of nitrogen and argon stable isotopes are constant over long periods in the atmosphere, $> 10^5 years$ [16] [17]. Due to both gases being relatively inert, they are useful in paleoclimatic research as proxies for the temperature gradient in the firn column and on the thickness of the diffusive column. These parameters can be calculated using measured $\delta^{15}N$ and $\delta^{40}Ar$ values and firn modelling [6].

Constituent[a]	Molecular weight	Fractional concentration by volume
Nitrogen (N_2)	28.013	78.08%
Oxygen (O_2)	32.000	20.95%
Argon (Ar)	39.95	0.93%
Water vapor (H_2O)	18.02	0–5%
Carbon dioxide (CO_2)	44.01	380 ppm
Neon (Ne)	20.18	18 ppm
Helium (He)	4.00	5 ppm
Methane (CH_4)	16.04	1.75 ppm
Krypton (Kr)	83.80	1 ppm
Hydrogen (H_2)	2.02	0.5 ppm
Nitrous oxide (N_2O)	56.03	0.3 ppm
Ozone (O_3)	48.00	0–0.1 ppm

Table 2.2: Volume fractions of the major gases in the Earth's atmosphere taken from [18]. Molecular weight is in $\frac{g}{mol}$.

2.5 Fractionation processes

As previously described, isotopic fractionation occurs in the diffuse zone of the firn layer. In the following, the two major fractionation processes are described. Understanding the physical and chemical processes of fractionation is necessary to model past climate parameters, such as site temperature, snow accumulation and firn column width.

2.5.1 Gravitational fractionation

Gravitational fractionation leads to an enrichment of the heavier isotopes with depth. According to[19] and [20], the gravitational settling or enrichment happens in the diffusive zone and can be calculated from the barometric equation [2]:

$$p(z) = p_0 e^{\frac{-Mgz}{RT}} \tag{2.6}$$

where p is the pressure at depth z, p_0 is the initial pressure, M is the molar mass, g is the gravitational acceleration, R is the ideal gas constant and T is the temperature. For a dual gas system with gas a and b, the ratio between their gravitational settling becomes:

$$R_{a,b}(z) = \frac{p_{0,a}}{p_{0,b}} e^{\frac{-\Delta Mgz}{RT}} \tag{2.7}$$

where ΔM is the difference of molar mass between gas a and b. Getting the ratio between the top of the firn column at $z = 0$ to some bottom depth level z:

$$\frac{R_{a,b}(z)}{R_{a,b}(z=0)} = e^{\frac{-\Delta Mgz}{RT}} \tag{2.8}$$

Using the delta notation from equation 2.3 the change of the gravitational settling can be calculated by:

$$\delta X_{grav}(z) = \left(e^{\frac{-\Delta Mgz}{RT}} - 1 \right) \approx \frac{\Delta Mgz}{RT} \tag{2.9}$$

A first order Taylor approximation is conducted to derive the last term in equation 2.9.

2.5.2 Thermal fractionation

When a temperature gradient is present in the firn column, the gas in the diffusive zone tends to unmix on a molecular level, called thermal diffusion. This temperature gradient will usually be caused by an abrupt change in the surface temperature since the bottom temperature reacts slowly. When the gas mixture is exposed to a temperature gradient, thermal diffusion will cause the heavier isotopes to move towards the colder region of the temperature gradient and the light isotope to move towards the warmer. The thermal fractionation is given in delta notation in the following equation: [21] [2] [3]:

$$\delta X_{therm} = \left(\left(\frac{T_s}{T_b} \right)^{\alpha_T} - 1 \right) \approx \Omega_T \Delta T \tag{2.10}$$

where

$$\frac{R_b}{R_s} = \left(\frac{T_s}{T_b} \right)^{\alpha_T} \tag{2.11}$$

and

$$\Omega_T \approx \frac{\alpha_T}{T_{mean}} \tag{2.12}$$

R is the ratio between two isotopes, T_{mean} is the mean firn temperature, α_T is the temperature-dependent thermal diffusion factor, s denotes the surface and b denotes the bottom of the firn column. ΔT is the temperature gradient between the top and bottom of the diffusive firn column, Ω_T is the thermal diffusion sensitivity. Ω_T and α_T are molecule dependent and have been experimentally derived [22] [23].

2.6 Mass spectrometry

Mass spectrometry is a scientific technique for analyzing the mass of ions in a mixture of gas, liquids or solids. This has numerous uses in many different fields, such as geology, geophysics, biology and pharmaceutics, where measurements of the isotopic composition of a given mixture are required. Mass spectrometry separates the gas compounds based on their mass to charge ratio, and a mass spectrum is obtained [24]. The invention of the first mass spectrometer is by most credited to Sir John Joseph Thomsen in 1897, who was also the discoverer of the electron by indirectly measuring its mass [25]. The mass spectrometer used in this study is a Delta V Plus Isotope Ratio mass spectrometer from Thermo Fischer Scientific. The mass spectrometer has two inlets for sample flow. The inlets are controlled by change-over valves. This allows for a quick change between two different gases entering the mass spectrometer and is useful for finding delta values of a sample by using a controlled reference gas. The following section describes the basic theory behind mass spectrometry.

2.6.1 Theoretical background

An illustration of the atom and molecule path from entering to being measured in the mass spectrometer can be seen in figure 2.2.
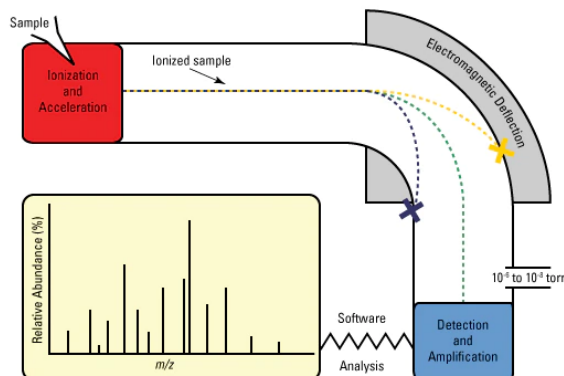
Figure 2.2: Simple diagram of how a mass spectrometer works. The particle or molecule enters the source and becomes ionized, it is accelerated forward into a magnetic field changing the its path, dependent on the path the ionized particle or molecule is detected in a Faraday cup where an electrical signal is measured and amplified, the mass to charge signal can be read from the Isodat software. Diagram taken from [24].

Gas is introduced into the mass spectrometer through capillary to an evacuated ionization chamber. The gas flow is determined by a pressure gradient between the outside controlled pressure of the line and the pressure inside the vacuum chamber. The flow rate is constrained by the inner diameter and length of the capillary connected to the inlet. The vacuum inside the mass spectrometer is in the order of $10^{-8}mbar$ without gas flow into the ionization chamber. In the ionization chamber, a part of the introduced atoms and molecules of the sample gas is ionized by a bombardment of electrons released by a heated tungsten filament. An ionized atom or molecule has ideally lost one electron and thus has a charge of $+1e = +1, 6 \cdot 10^{-19}C$. The ionized atoms or molecules are accelerated in a chamber with an electric field created by a voltage difference of several kV and enters a homogeneous magnetic field created by an electromagnet. The electromagnetic field is perpendicular to the velocity vector of the ionized molecules, and they are deflected on a circular trajectory with a radius depending on their mass to charge ratio. The trajectories determine where the detector cups are located. The kinetic energy of the ionized particle can be described by the product of the voltage difference creating the electric field for the acceleration and the charge of the particles accelerated [9]:

$$Uq = \frac{1}{2}m\mathbf{v}^2 \tag{2.13}$$

where U is the voltage difference, q is the charge, v is the velocity of the ionized particle and m is the mass of the particle. Isolation of v leads to:

$$v = \sqrt{\frac{2Uq}{m}} \tag{2.14}$$

The deflection of the particles due to the magnetic field can be derived from the Lorentz force and the centripetal force:

$$\mathbf{F} = q\mathbf{v} \times \mathbf{B} = \frac{m\mathbf{v}^2}{r} \tag{2.15}$$

where $\mathbf{F}$ is the force vector, $\mathbf{B}$ is the magnet field vector and r is the curvature path. Isolating for r and assuming constant acceleration voltage and magnetic field strength gives:

$$qvB = \frac{mv^2}{r} \tag{2.16}$$

$$r = \frac{mv}{qB} \tag{2.17}$$

Substitution of equation 2.14 into equation 2.17 leads to:

$$r = \frac{1}{B}\sqrt{\frac{2mU}{q}} \tag{2.18}$$

From equation 2.18 it can be seen that r is dependent on the mass to charge ratio $\frac{m}{q}$ given a constant magnetic field and voltage potential. For a larger mass to charge ratio, the particles will take a trajectory with a larger radius.

The deflected charged particles are detected when they hit the Faraday cups.

The ion statistics, that causes the voltage signal measured from the Faraday cups, are described in the following. N is the number of molecules per second that enters the source, M is the number of molecules per ion, n is the number of ions per second detected in the Faraday cups. N, n and M are related by $n = \frac{N}{M}$. The ion current I is the product of n and the elementary charge e^- so $I = ne^-$. Combining this with Ohm's law [26]:

$$U = RI \tag{2.19}$$

N can be calculated from the gas flow into the ion source determined by a capillary. The volume moving through the capillary in a certain time can be denoted: V' $[\frac{ml}{min}]$. The ideal gas law is given as [27]:

$$pV = Nk_bT \tag{2.20}$$

where p is the pressure, V is the volume, N is the number of molecules, k_b is Boltzmann's constant and T is the temperature. For a constant pressure p_0 and temperature T_0, the ideal gas law can be solved for N:

$$N = \frac{V'P_0}{k_bT_0}\epsilon \tag{2.21}$$

where ϵ is the fraction of the measured compound of the total gas mixture. For a pure gas entering the mass spectrometer $\epsilon = 1$, for nitrogen in air $\epsilon \approx 0.79$. Combining 2.21 with $I = \frac{N}{M}e^-$ and Ohms law, the voltage at the Faraday cup is found:

$$U = R\frac{N}{M}e^- = R\frac{1}{M}e^-\frac{V'p_0}{k_bT_0}\epsilon \tag{2.22}$$

The ion current creating the voltage from equation 2.22 is integrated over a period of time, and the current is measured with a resistor and amplified into a voltage signal. This voltage signal can be read with software such as Isodat [28]. The signals precision is in the order of hundreds of mV. The amplification is determined by the different resistors converting the ion current into voltage. The resistors are chosen in a way that they match with the abundances of the isotopes to give measurable signals. Every mass spectrometer has a cup configuration specifically made to measure certain masses. The mass spectrometer used for the measurements in this thesis has 11 faraday cups. A description of the molecules or isotopes from air measured in their respective cup can be seen in table 2.3.

Mass	28	29	30	32	36	40	44
Molecule or isotope	$^{14}N^{14}N$	$^{14}N^{15}N$	$^{14}N^{16}O$	$^{16}O^{16}O$	$^{18}O^{18}O, ^{36}Ar$	^{40}Ar	$^{12}C^{16}O^{16}O$

Table 2.3: The molecular masses measured on the air configuration and the most likely molecules or isotope measured.

Some of the cups have multiple resistors so that the amplification can be switched between the high and low amplification settings in Isodat Instrument Control. The specific cup configuration used for the measurements of this thesis is shown in figure 2.3.
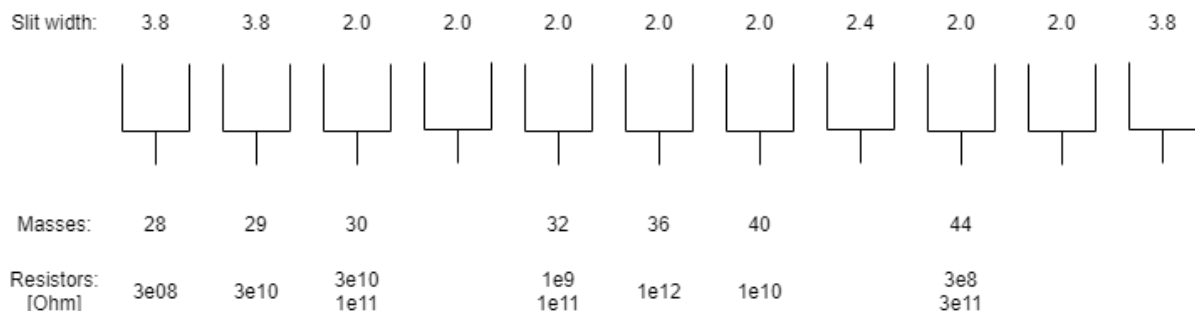
Figure 2.3: An illustration of the specific cup configuration inside the mass spectrometer used in my experiments. The 11 cups are shown with their respective slit width in mm, measured mass in $\frac{q}{m}$ and the resistors in Ω.

It has to be mentioned that the detection cups cannot differentiate between particles of similar mass to charge ratios. As such, different isotopes of similar mass to charge ratios are being detected in the same cup. When measuring $\delta^{40}Ar$ from atmospheric air, the main problem is the barometric interference of $^{18}O^{18}O$ and ^{36}Ar have the same mass to charge ratio. There might also be a power from fragmentation of CO_2 into $^{12}C^{16}O$. It has been shown that nitrogen and oxygen can react inside the ion source to form N_2O and nitric oxides, such as NO and NO_2 [29]. This might cause additional fractionation on the $\delta^{15}N$, and in general, deplete the measured nitrogen signal. Hence removing oxygen from the sample stream is a good idea before it enters the ion source. One of the main objectives of this thesis is to investigate strategies for removing the oxygen with a perovskite membrane, as well as removing the majority of the carbon dioxide by freezing it with liquid nitrogen to prevent changes of the δ values occurring inside the mass spectrometer.

2.6.2 Resolution of a mass spectrometer

For a Delta V plus mass spectrometer, the mass resolution R is defined as the ratio between the ion mass m and the ion mass difference of two neighboring peaks Δm if the valley between peaks drops to 10 % of the peak height. [9][30]:

$$R = \frac{m}{\Delta m} \qquad (2.23)$$

The resolution describes which masses can be distinguished from each other based on the 10% valley definition. Since the intensity peaks depend on the width of the ion beam and the width of the slits, so does the resolution. The ion beam can be controlled with the focus settings in the software Isodat.

2.6.3 Isodat

The software used for Thermo Fischers mass spectrometers is called Isodat NT [28]. The version installed was Isodat 3.0. Isodat allows control and configuration of the mass spectrometer to optimize the measurements. There are several subprograms installed with Isodat. Instrument control lets you monitor and control key parameters and run several different scans to measure, test and monitor the signal intensities for the different gas compounds. Acquisition lets you run sequence files, method files and ISL scripts. The sequence file enables the user control measurements, how they should be run and which pre-measurement corrections should be applied[30]:

- Peak center: Finds the middle of the peak by changing the high voltage accelerating the particles until a stable large signal is achieved on the respective cups.

- Background: Measures the background without any sample and zeros all the intensities.

- Pressure Adjust: Adjust the pressure in the bellows (not used in this work where a continuous sample stream is used).

- Method: Lets you chose which method should be used for each specific measurement.

The method file controls the following:

- ISL script: Controls the mass spectrometer functions during a measurement, e.g. the turn over valves which switches between the reference and sample inlet.

- Cup configuration: Chose between configurations. This depends on which sample gas is introduced and which isotopes are supposed to be measured.

- Integration time of each measurement. A longer integration time reduces the random noise by integrating over a longer period.

- Peak center settings.

- Cycles: Control how many cycles are used. One cycle consists of 3 measurements. First, the reference is measured, lets call this R_1. Secondly, the sample is measured, lets call this S_1. Thirdly, the reference is measured again, lets call this R_2. From each cycle, a ratio between the sample and reference can be found. The method calculates the ratio with the S_1 average of R_1 and R_2. Every cycle subsequent to the first only does two measurement one on the reference side and one sample side. For calculating next ratio it uses R_2 of the previous ratio measurement as R_1 in the next.

- Idle time: Time between measurements. Required to let the source reach an equilibrium after the reference and sample has switched.

- Background: Controls the settings for the background.

- Evaluation of δ values are done.

Workspace lets you visually analyze and export scan or acquisition data. Version handler allows you to go back to a previously installed configuration of Isodat if the current version becomes corrupted. Isodat is an old program and not optimized for windows 10. A corruption of the software files occurred on multiple occasions, and the version handler was used to reinstall a version, which was saved after a clean installation. Isodat Configuration enables you to configure the Isodat GUI, setup the mass spectrometer hardware and how it communicates with the control computer.

Two different approaches to measure and calculate the δ values were used in this work. The first method was monitoring the mass intensities with a time scan. From the raw signal intensities, δ values were calculated manually. A reference was chosen manually by averaging the measured intensities over a certain time period, usually the first period. The samples were all compared to the manually chosen reference.

The second option was through the Isodat Acquisition. The acquisition calculates δ values by automatically switching between a reference and sample gas and outputs the average δ value along with its standard deviation and standard error.

2.6.4 Ion source and focus settings

If the high voltage delivered to the ion source is unstable, it will result in unstable ionization and ion acceleration, and thus the measured mass intensities will oscillate. A problem occurred where the high voltage was oscillating between $2.85 - 3.25 KV$. To fix this, a visual inspection of the ion source was done to make sure there were no broken dust or ceramic pieces because even small changes in the geometry of the ion source can influence the ion beam, and thus the measurements. When the source was taken in and out, the focus settings of the ion beam have to be refocused. To do that, Isodat Instrumental Control has an automated focusing setting which slightly changes the direction of the ion beam before entering the magnetic field in order to maximize the signal intensities. This is achieved by changing the electric field strength by changing the voltage difference on a

series of focusing plates in the ion source. The focus setting parameters can also be manually controlled. They include: Emission, trap, electron energy, extraction, extraction symmetry, X-Focus, X-Focus Symmetry, X-Deflection, Y-Deflection, Y-Deflection symmetry, Focus Quad and SE-Supression. However, the problem was found to be the high voltage control board. The board was swapped with one from a Delta V Advantage mass spectrometer. Here a description of the process is made since it required the removal of the normal safety barriers of the mass spectrometer circuit board. The first step was to remove high voltage power after turning off the mass spectrometer. The second step was to remove the protective plastic plate. The third step was to visually inspect all the capacitors and fuses. The fourth step was the removal of the approximately 40 wires and noting their location. The fifth step was to remove all screws which kept the control circuit board attached to the mass spectrometer. The sixth step was to remove the high voltage control board. Changing the high voltage control board with the one from the Advantage mass spectrometer fixed the oscillating high voltage. In figure 2.4
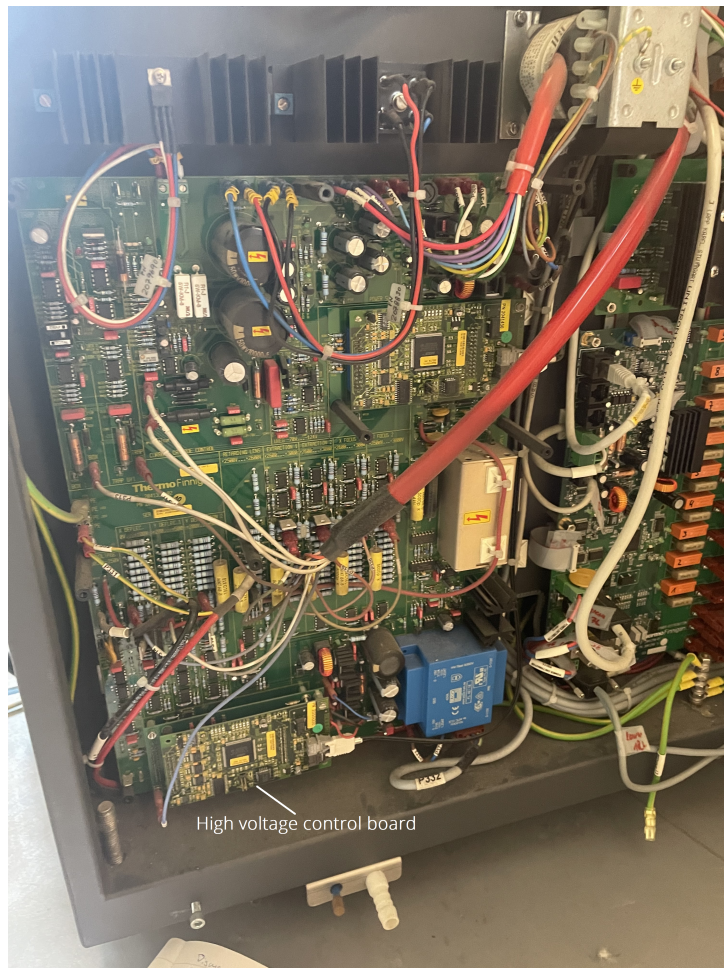
Figure 2.4: Picture taken of the electronics board in the back of the mass spectrometer. Picture taken after removing protective plastic. Two arrows have been included, one points to the ion source controller board which was replaced, one points to a group of the capacitors

Before beginning measurements, the tungsten filament was changed in addition. It

deteriorates over time since it provides electrons for the ionization process when a current generated by the high voltage is run through it. The state of the filament can be observed in the instrument control by the trap current and the box current. When the filament parameters begin to diverge, it is a sign that the filaments need to be changed. This was done once during the scope of this thesis.

2.7 Data corrections

When measuring with a mass spectrometer, the raw data will be subjected to several instrumental errors. This section describes corrections applied to transform the raw data into presentable results.

2.7.1 Background correction

When a sample is introduced into the mass spectrometer, some remnants remain even after the valves have been closed off. The stickiness of molecules is different, and especially NO (mass 30) and CO_2 (mass 44) remain in the source for a relatively long amount of time. To correct for the background, a measurement of the intensities with both inlet valves closed is subtracted from the mass intensities. This can be done manually by measuring with both inlets closed through Isodat Instrument Control or the setup of an acquisition run. The background correction is described by:

$$I_{bgc} = I_{measured} - I_{bg} \tag{2.24}$$

where I is the intensity, bgc is background corrected, bg is background.

2.7.2 Zero enrichment correction

The zero enrichment test verifies the stability of the measurement of isotope ratios [31][32]. It reveals if the sample or reference undergoes fractionation in their respective lines. It works by introducing the same gas into both sample and reference inlet. The measured isotopic ratios should be equal. This test reveals if there are any precision errors in the instrument or in the line. Measurements can be corrected for this effect with the following equation:

$$\delta X_{Z.E.C} = \delta X_{raw} - \delta X_{Z.E.M} \tag{2.25}$$

where $Z.E.C$ is the measured δ corrected for the zero enrichment, δX_{raw} are the δ values obtained from the raw signal intensities and $\delta X_{Z.E.M}$ is the offset found by the zero enrichment measurement.

2.7.3 Pressure imbalance

The ratio between different mass intensities is sensitive to changes in the flow. Since the flow from the reference and sample are not identical, the measured ratios will be slightly

different, and in turn, the calculated δ value is affected. When measuring from only one inlet and when there are small changes in the flow, the measured δ values will be affected by the flow change, and a correction must be applied. Similarly, a correction needs to be made when using both the sample and reference inlet because the flows are not identical. The pressure imbalance has been found to vary in time, and other studies have done the test on a weekly basis [32].

The pressure imbalance is found by varying the pressure gradient between inside and outside of the mass spectrometer and hence the flow into the source. The change in the δ values is measured, and a linear fit to the measured δ values is calculated. The pressure imbalance effect is determined from the slope of the fit, and measurements can be corrected for this effect. This correction is applied after the zero enrichment correction. To correct a measurement, the slope is multiplied with the difference in voltage between the sample and the reference subtracted from the zero enrichment corrected δ. This is described by the following equation:

$$\delta X_{P.I.C} = \delta X_{Z.E.C} - \alpha_{P.I} \cdot (I_{Xsample} - I_{Xreference}) \tag{2.26}$$

where $P.I.C$ is the pressure imbalance correction, α is the slope, $int_{X_{sample}}$ and $int_{X_{reference}}$ is the mass intensity of the most abundant isotope, e.g., for $\delta^{15}N$, the intensities are from mass 28.

2.7.4 Chemical slope correction

The measured isotopic ratios in the source are sensitive to changes in the composition of the gas. This means that the $\delta^{15}N$ is sensitive to changes in the relative abundance of nitrogen, oxygen and argon. This effect happens in the source due to changes in the ionization efficiency of the isotopes [16]. To correct for this effect, the δ values are obtained with a pure gas added to the sample. Measuring with several levels of the pure gas allows for the effect on the δ value to be calculated. Then, a linear fit can be calculated, and the measurement data can be corrected for this effect. This is done after the pressure imbalance correction. The chemical slope correction is described by:

$$\delta X_{C.S.C} = \delta X_{P.I.C} - \alpha_{C.S}\delta\frac{Ar}{N_2} \tag{2.27}$$

where $C.S.C$ is the chemical slope correction. When calculating the chemical slope for $\delta^{15}N$, pure argon is introduced, and for $\delta^{40}Ar$ pure nitrogen is introduced.

2.7.5 Uncertainty on the measurement

The uncertainty on the raw signal intensities is mostly due to electrical noise and is calculated by the standard deviation [33]:

$$\sigma_x = \sqrt{\frac{1}{N}\sum_i (x_i - \bar{x})^2} \tag{2.28}$$

where σ is the uncertainty, N is the total number of measurements, x is the signal intensity, i is the i'th measurement, $\bar{x}$ is the mean value of the signal intensities. The standard error of the mean is obtained by:

$$\sigma_{\bar{x}} = \frac{\sigma_x}{\sqrt{N}} \tag{2.29}$$

The uncertainty on the δ values is obtained from Gaussian error propagation. The uncertainty is propagated through every correction [33]:

$$\sigma_f^2 = \left(\frac{\partial f}{\partial x_1}\right)^2 \sigma_{x_1}^2 + ... + \left(\frac{\partial f}{\partial x_n}\right)^2 \sigma_{x_n}^2 \tag{2.30}$$

where f is some function, σ is the uncertainty, x_1 is the first variable of f, x_n is n'th variable of f. The uncertainty on the ratio between two isotope mass intensity A and B is obtained by:

$$\sigma_{R_{\frac{A}{B}}}^2 = \left(\frac{1}{I_B}\right)^2 \sigma_A^2 + \left(-\frac{I_A}{I_B^2}\right)^2 \sigma_{I_B}^2 \tag{2.31}$$

The error propagation on the delta value, where the sample components are denoted I_A and I_B and the reference components are denoted I_C and I_D, can be calculated as:

$$\sigma_\delta^2 = \left(\frac{I_D}{I_B I_C}\right)^2 \sigma_{I_A}^2 + \left(-\frac{I_A I_D}{I_B^2 I_C}\right)^2 \sigma_{I_B}^2 + \left(-\frac{I_A I_D}{I_B I_C^2}\right)^2 \sigma_{I_C}^2 + \left(\frac{I_A}{I_B I_C}\right)^2 \sigma_{I_D}^2 \tag{2.32}$$

The error propagation on the corrections can likewise be found, first shown for the zero enrichment correction, secondly shown for the pressure imbalance and thirdly for the chemical slope correction:

$$\sigma_{\delta_{Z.E.C}}^2 = \sigma_{\delta_{raw}}^2 + \sigma_{\delta_{mean}}^2 \tag{2.33}$$

$$\sigma_{\delta_{P.I.C}}^2 = \sigma_{\delta_{Z.E.C}}^2 + \left(-I_{Xsample} + I_{Xreference}\right)^2 \sigma_{\alpha_{P.I}}^2 + \alpha_{P.I}^2 \sigma_{I_{Xsample}}^2 + \alpha_{P.I}^2 \sigma_{I_{Xreference}}^2 \tag{2.34}$$

$$\sigma_{\delta_{C.S.C}}^2 = \sigma_{\delta_{P.I.C}}^2 + \left(\delta \frac{Ar}{N_2}\right)^2 \sigma_{\alpha_{C.S}}^2 + \alpha_{C.S}^2 \sigma_{\delta \frac{Ar}{N2}}^2 \tag{2.35}$$

The amount of electrical noise is dependent on the resistor that amplifies the measured mass signal. Because of this, the electric noise is larger for the minor isotopes where the mass signal has been amplified. Therefore, in the error propagation, it is the minor isotopes that will dominate the terms. From the manual calculation of the δ values, the uncertainty on the δ values can also be calculated using equation 2.28.

2.8 Continuous flow analysis

One of the purposes of this thesis is to reconstruct the continuous flow analysis setup used by David Soestmeyer and Jesper Baldtzer Liisberg in the DYE-3 campaign. Their work is a continuation of NEEM, RICE and RENLAND campaigns[17].

Two primary methods are utilized to analyze gas from ice cores, continuous flow analysis and discrete sampling. In discrete sampling, an ice sample with a length of approximately $10 - 40cm$ [2] is prepared and continuously melted. Each measurement section of the ice core has to be manually cut. The extracted gas can now be stored, and the bellows can be filled. For continuous flow analysis, each ice core section can be stacked on the last one [17] allowing for more measurements in the same amount of time. However, continuous flow analysis generally requires a more complex measurement system. There are more places where complications in the measurement line can take place. Thus, continuous flow analysis is less accurate compared to discrete measurements. Since there were no ongoing measurement campaigns during the course of this thesis, the setup was never used in the way of a proper continuous flow analysis on gas extracted from melted ice. It was shown that it was stable over long periods of time and can be used for measuring stable isotopes of argon and nitrogen in a possible future measurement campaign.

2.9 Removal of unwanted components in sample air

One of the objectives when measuring $\delta^{40}Ar$ and $\delta^{15}N$ is to have as little as possible interference from other components of atmospheric air as explained in section 2.6 . This was achieved by removing oxygen with a perovskite membrane, removing carbon dioxide by freezing it with liquid nitrogen and removing water vapor with a nafion.

2.9.1 Oxygen removal

The mass spectrometer cannot differentiate between, e.g., $^{18}O^{18}O$ and $^{Ar}36$ as they are measured on the same cup. Since oxygen consists of approximately 20.95 % of atmospheric air, this will affect the mass to charge measurements of ^{36}Ar. To correct for this problem, the majority of the oxygen has to be removed from the sample stream. This method was tested and developed by Bianca Xuan Nguyen Larsen [34] and was used in the DYE-3 campaign [17]. The tool for removing oxygen was a tubular perovskite membrane obtained from the Fraunhofer-Institute for Interfacial Engineering and Biotechnology Inorganic Surfaces and Membranes. The oxygen removal is driven by a partial pressure difference between the outside and inside of the membrane, as can be seen in figure 2.5. In the sample stream, atmospheric air is transported into the membrane. On the outside of the membrane, there is no oxygen, only helium, which causes a partial pressure difference of oxygen. To avoid accumulation of oxygen, the outside of the membrane is continuously exposed to a carrier gas free of oxygen. In the results presented in this thesis helium was chosen. This caused the oxygen continually to be removed as the sample gas flowed through the membrane. The oxygen removal through the membrane was activated at temperatures of approximately $600\,°C$ with the highest degree of removal at temperatures between 850-950 $°C$ [17]. To achieve this, a custom-built oven was made, and a quartz glass tubing was used to place the membrane and control the helium flow. Quartz glass was chosen due to its melting point of $1650°C$. Earlier experiments found oxygen removal

rates as high as 99.8 % [34] [17]. It should be noted that they worked with a slightly different oven setup. One of the objectives of this thesis was to replicate the removal rate with a new setup consisting of a smaller oven.
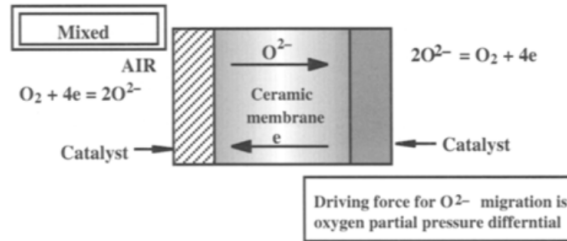
Figure 2.5: Sketch of how oxygen removal is driven by partial pressure difference between the outside and inside of the membrane. Schematic is taken from [35].

2.9.2 Carbon dioxide trap

Carbon dioxide is removed from the sample stream with a liquid nitrogen trap. This is achieved by letting the sample flow through a $\frac{1}{16}$" steel tubing, which was submerged into liquid nitrogen. Liquid nitrogen has a temperature of -196 °C, which causes the carbon dioxide to freeze due to its freezing temperature of -78.5 °C. This leaves the carbon dioxide frozen in the line. Carbon dioxide was removed due to the fragmentation and reaction potential previously described.

2.9.3 Water removal

For a campaign measurement, ice is melted with the help of a melt head. Gas and water are separated with a micromodule, which leaves the gas more saturated with water vapor relative to atmospheric air. Fragmentation of the water molecules into oxygen and hydrogen can affect the isotopic δ values, thus water is removed. The sample gas is dried with a nafion, which works due to a partial pressure difference like the perovskite membrane. In this work, helium was used as a carrier gas to transport the removed water vapor away[17].
Atmospheric air from the NEEM ice core location was used as the sample gas, so the water vapor removal was not necessary for my measurements. However, it is needed for an actual measurement campaign.

2.10 Laminar pipe flow

During the building of the setup, many calculations were made on the flow rate of gases. The primary concern is calculating the approximate gas flow through the capillaries and the steel tubes, which were assumed to have the geometry of a cylindrical pipe. Pressure-driven laminar flow of fluids in a pipe is described by the Hagen-Poisueille law [27].

The fluid velocity in a pipe is derived by simplifying the Navier-Stokes equations under the assumption that the fluid is incompressible and only driven by a constant pressure difference between the entrance and exit of the pipe. This causes the acceleration of the fluid through the pipe to be zero. A simple sketch of a pipe can be seen in figure 2.6. Assuming that the velocity cannot be infinite at $r = 0$ and that the velocity at the boundaries must be 0, $v_z(a) = 0$, the differential equation can be solved and a specific solution can be derived called the Poiseuille solution. The result is velocity field of a fluid v through the pipe in the z direction:

$$v_z(r) = \frac{\Delta p}{4\eta L}(a^2 - r^2) \tag{2.36}$$

where v is the velocity field, a is the radius, r is the coordinate parallel to the radius of the pipe, $\Delta p = p(z = 0) - p(L)$ is the pressure change between entry and exit point of the pipe and η is the viscosity of the gas.

The volume of fluid per unit of time Q, in this thesis noted in ml per min $\frac{ml}{min}$, can be found by integrating the velocity field over the cross section of the pipe:

$$Q = \int_0^a v_z(r)2\pi r dr = \frac{\pi \Delta p a^4}{8\eta L} \tag{2.37}$$

Assuming constant geometry of the pipe, Q is linearly dependent on the pressure difference ΔP and inversely on the viscosity of the fluid. Whether or not the flow becomes turbulent is described by the Reynolds number:

$$Re = \frac{\rho_0 \Delta p a^3}{4\eta^2 L} \tag{2.38}$$

where ρ_0 is the density of the gas. Assuming constant geometry and density, the Reynolds number depends linearly on the pressure difference and inversely on the viscosity. The pipe flow is laminar at Reynolds numbers below approximately 2000-4000. Otherwise, the flow is non-linear and turbulent and does not behave according to equation 2.37 [27].
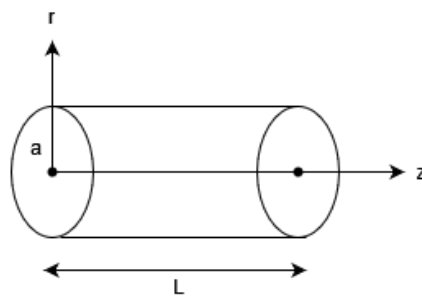
Figure 2.6: Illustration of a pipe. Pipe has length L, radius a,

2.11 Experimental Setup

The CFA setup was a continuation of the work done by David and Jesper in the DYE3 campaign. They built their work upon the campaigns measuring ice from NEEM, RICE

and RENLAND. The setup used in the DYE3 campaign can be seen in figure 2.7. The setup used in this thesis was rebuilt based on the point where the micromodule extracted the preserved gas from the melted ice. This can be seen in the lower right part of figure 2.7.
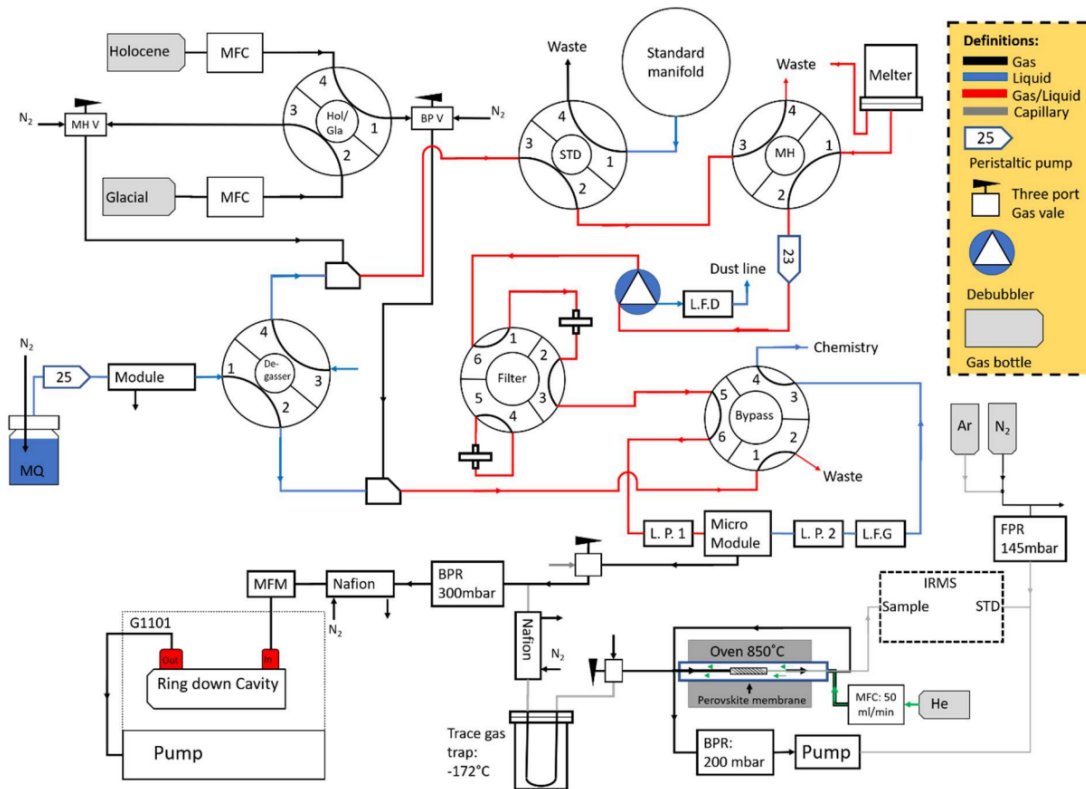
Figure 2.7: The overall setup from the DYE3 campaign, figure taken from [17].

The setup was rebuilt almost entirely from scratch because the setup was taken apart after the last measurement campaign. The setup was continually changed and tweaked while testing and building the setup.

While doing the zero enrichment correction, the pressure imbalance correction and the chemical slope correction, the setup in figure 2.8 was used. For simplicity, the reference and sample side of my final measurement setup is split into two figures. The reference side can be seen in figure 2.9, and the sample side can be seen in figure 2.10. Note, however, that they are both in use simultaneously. In the following, the flow of gas is described in the respective figures. When referring to directions, it is the direction in the respective schematic.

For the pressure imbalance correction, the setup in figure 2.8 was used. The flow begins in the upper left from a compressed gas bottle containing the reference gas consisting of a mixture of 98.8 % nitrogen and 1.2 % argon. The flow is controlled with a pressure controller set to 3.5 bar over pressure. From the compressed gas bottle the gas flows through a steel tube to a flow controller. Here flow could be adjusted with the flow controller to reduce excess use. The flow controller was connected to a cross. On the

right part, a steel tube was connected to an on-off-valve open to the room air. This was needed for the forward pressure regulator to be able to regulate the pressure.

In the cross, the flow splits through the top and bottom connection. The top of the cross was connected to the three point valve with a capillary. The bottom part of the cross was connected to a particle filter and the flow went through the forward pressure regulator via a steel tube. A t-split was connected to the forward pressure regulator. The bottom part of the t-split sends the flow into the reference side of the mass spectrometer. The left part of the t-split was connected to a vacuum pump with a pneumatic plastic tube. The forward pressure regulator is used to control the flow through a pressure gradient to the mass spectrometer.

The three point valve was used as on off valve with the bottom side closed with a cap. The left side was connected with a capillary to a cross with a capillary. The top of the cross was closed with a cap when doing the pressure imbalance measurements. The bottom of the cross was connected to a backward pressure regulator with a steel tube and was connected to a vacuum pump with a plastic tube. The backward pressure regulator controls the pressure gradient driving the gas into the sample side of the mass spectrometer. The sample flowed into the mass spectrometer from a capillary connected to the left of the cross. Both the forward pressure regulator and the backward pressure regulator were controlled digitally with the software LabVIEW.

The same setup was used for the zero enrichment correction.

The setup for the chemical slope was similar. However, from the top of the cross next to the mass spectrometer sample inlet, the flow on the sample line came from a gas volume filled with gases needed for the respective chemical slope corrections. The volume capillary length was calculated to increase the amount of the respective gases by a certain percentage but still to be within the upper bound of the signal intensities, which was $50V$. The introduced gases were pure nitrogen, argon, CO2 and oxygen.

The reference line from the final setup is the same as the correction setup. In the sample line, the flow begins from the sample gas container filled with NEEM air and connected to a pressure controller. The gas flows through a capillary to a t-split. The right side of the t-split is connected to a three point valve with a small steel tube. The three point valve functions as an on-off valve with the right side capped. The bottom is connected to a vacuum pump with a pneumatic plastic tube. The function of the three point valve was to evacuate the line. From the t-split, the gas flows through the bottom part into the nafion with a capillary.

In the nafion, water vapor is removed from the sample. The nafion was wrapped around two thicker capillaries and placed inside a $\frac{1}{16}$" steel tube. The nafion was prepared by submerging it in alcohol, causing the nafion to expand. Then, the ends were slid into two capillaries, and the nafion was heated with a heat gun, causing it to shrink again.

In the steel tube, the nafion was placed inside, a flow of helium of $5\frac{ml}{min}$ streamed in the opposite direction of the gas flow. Through a short open split, the helium and removed water vapor was evacuated through the pump into the room. The helium flow was controlled by an analog mass flow controller.

From the nafion, the sample gas flowed through a capillary connected to a steel tube. The steel tube was submerged into a dewar filled with liquid nitrogen, where the carbon dioxide was frozen. The right side of the carbon dioxide trap is connected to a cross with double holed graphite-vespel ferrule. The gas flows into the end of a perovskite membrane resting inside a quartz tube going through the oven. The perovskite membrane was sealed with gold paste. The gas moves through the membrane and part of it into the capillary, that goes through the second hole in the double holed ferrule, into the mass spectrometer. In the top part of the cross at the oven, an over pressure valve was installed to avoid a potential pressure build in the reactor quartz tube. The bottom part was connected to a back pressure regulator, which through a pneumatic plastic tube was connected to a vacuum pump. The left side of the cross at the oven was attached to the right side of the reactor quartz tubing with an Ultra-Torr vacuum fitting. The left side of the reactor quartz tube was connected with both an Ultra-Torr vacuum fitting and a normal swagelok nut during the measurements. This was to test if the O-ring was releasing oxygen and carbon dioxide or if it became permeable to air due to being heated.

From the left side of the oven ran a helium stream to remove the oxygen transported through the perovskite membrane. The helium was controlled by a manual flow controller and a digital flow meter. The oven was heated by a heating wire coiled around a quartz tube and sealed with chemical cement. The heating wire was powered and controlled by a DC power supply. The oven temperature was observed by a k-type thermocouple located between the reactor quartz tube and heating quartz tube. The thermocouple was connected to a quantrol lc100, which displayed the temperature.

With the combined setup of the reference and the sample side, Isodat Acquisition could be used to measure a reference gas and a sample gas.
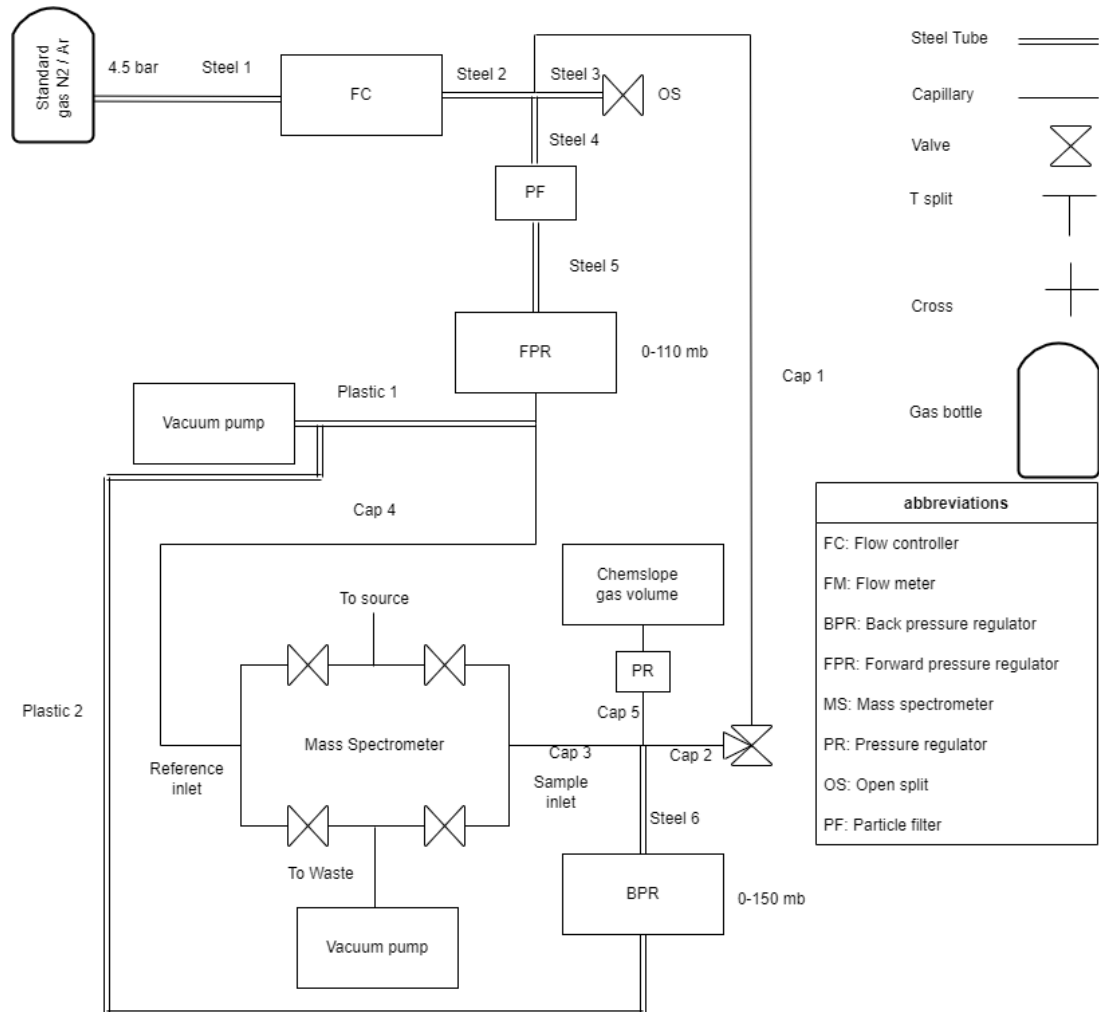
Figure 2.8: A schematic of setup used for the correction measurements. A description of the included components is presented here. The steel tubes are of stainless steel, and their dimension are described with outer diameter OD and length L. Steel 1: $\frac{1}{8}$", $L \approx 8m$. Steel 2: $\frac{1}{16}$", $L \approx 2m$. Steel 3: $\frac{1}{16}$", $L \approx 60cm$. Steel 4 is connection between the particle filter and the $\frac{1}{16}$" cross. Steel 5: $\frac{1}{8}$", $L \approx 0.5m$. Steel 6: $\frac{1}{16}$", $L \approx 0.5m$. Plastic 1 and Plastic 2 are pneumatic plastic tubing from Festo, swaged with a $\frac{1}{4}$" brass ferrule, used to connect a vacuum pump (Pfeiffer DUO 3 M) to the forward pressure regulator (Bronkhorst El press Flow-bus) and the back pressure regulator(Bronkhorst El Press @Digital). The capillary tubes are of the type TSP FS, standard polyimide coating fused silica, they are described by their inner diameter ID, outer diameter OD and length L. Cap 1: $ID = 100\mu m$, $OD = 238\mu m, L = 155cm$. Cap 2: $ID = 50\mu m$, $OD = 238\mu m, L = 40cm$. Cap 4: $ID = 100\mu m$, $OD = 363\mu m, L = 114cm$. Cap 4: $ID = 100\mu m$, $OD = 238\mu m, L = 114cm$. Cap 4: $ID = 100\mu m$, $OD = 238\mu m, L = 114cm$. Three different capillaries was used for Cap 5, one for each of the introduced gasses for the chemical slope. Cap 5 for added nitrogen: $ID = 20\mu m$, $OD = 375\mu m, L = 54cm$. Cap 5 for added nitrogen: $ID = 5\mu m$, $OD = 150\mu m, L = 13cm$. Cap 5 for added carbon dioxide: $ID = 10\mu m$, $OD = 150\mu m, L = 50cm$. The Flow controller (Porter flow controller, model VCD 1000) has a range of $\approx 0 - 60\frac{ml}{min}$. The particle filter was a Swagelok Inline Welded Particulate Filter. The mass spectrometer was a Delta V plus from Thermo Fisher Scientific connected to a vacuum pump (Pfeiffer DUO 3 M). The Chemslope gas volume, was made from a $\frac{1}{4}$" tubing between 2 Swagelok valves.
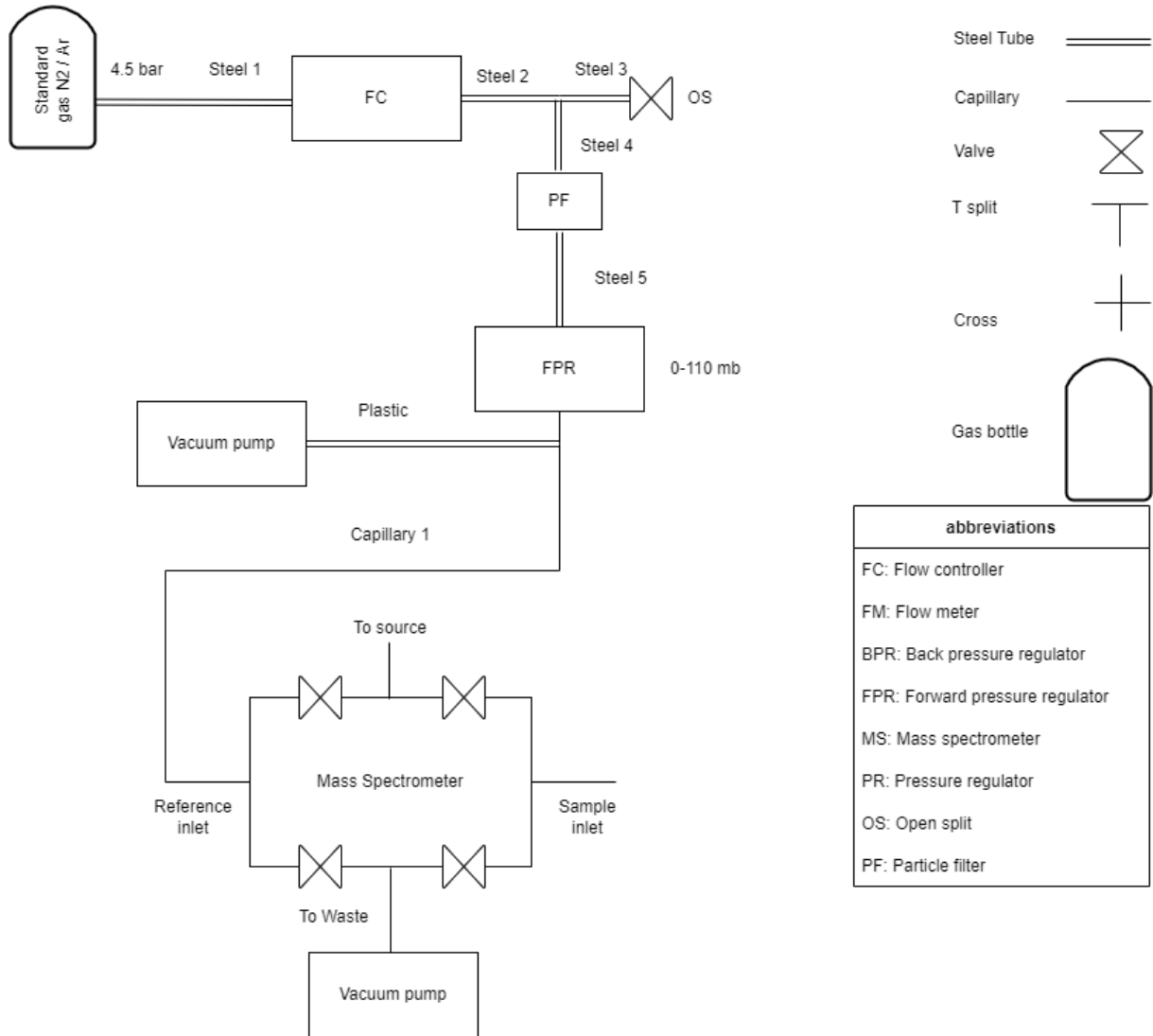
Figure 2.9: A schematic of the reference side of the setup. A description of the included components is presented here. The steel tubes are of stainless steel, and their dimension are described with outer diameter in inches " and length L. Steel 1: $\frac{1}{8}$", $L \approx 8m$. Steel 2: $\frac{1}{16}$", $L \approx 2m$. Steel 3: $\frac{1}{16}$", $L \approx 60cm$. Steel 4 is connection between the particle filter and the $\frac{1}{16}$" cross. Steel 5: $\frac{1}{8}$", $L \approx 0.5m$. Plastic 1 is a pneumatic plastic tubing swaged with a $\frac{1}{4}$" brass ferrule, used to connect a vacuum pump (Pfeiffer DUO 3 M) to the forward pressure regulator (Bronkhorst El press Flow-bus). The capillary tube are of the type TSP FS, standard polyimide coating fused silica, they are described by their inner diameter ID, outer diameter OD and length L. Capillary 1: $ID = 100\mu m$, $OD = 238\mu m$, $L = 114cm$. The Flow controller (Porter flow controller, model VCD 1000) has a range of $\approx 0 - 60\frac{ml}{min}$. The particle filter is a Swagelok Inline Welded Particulate Filter. The mass spectrometer is a Delta V plus from Thermo Fisher Scientific connected to a vacuum pump (Pfeiffer DUO 3 M).
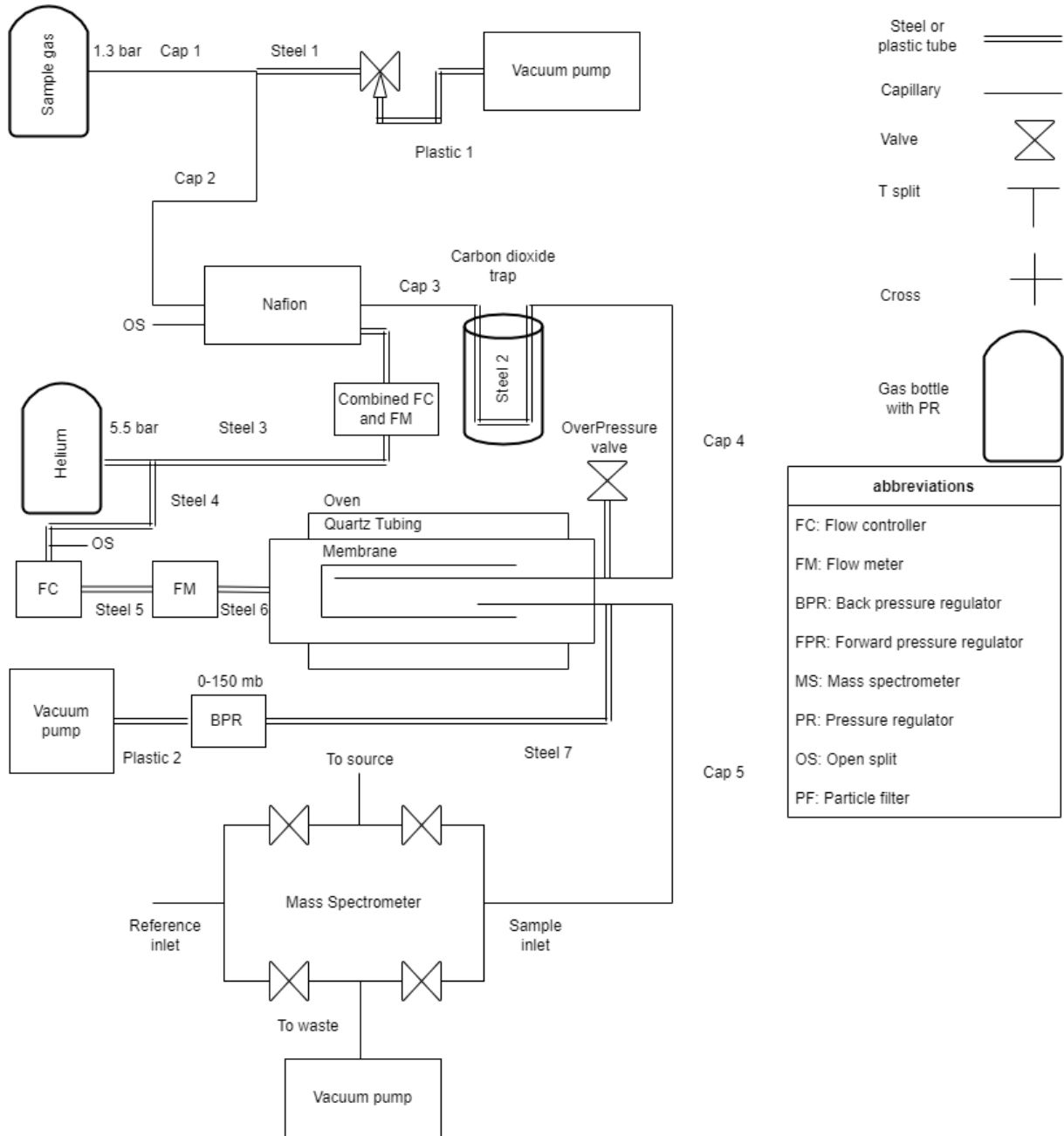
Figure 2.10: A schematic of the sample side of the setup. A description of the included components are presented here. The steel tubes are described with outer diameter in inches " and length L. Steel 1: $\frac{1}{16}$", $L \approx 5cm$. Steel 2: $\frac{1}{16}$", $L \approx 40cm$. Steel 3: $\frac{1}{8}$", $L \approx 8m$. Steel 4: $\frac{1}{8}$", $L \approx 8m$. Steel 5: $\frac{1}{8}$", $L \approx 2.5m$. Steel 6: $\frac{1}{16}$", $L \approx 40cm$. Steel 7: $\frac{1}{4}$", $L \approx 15cm$. Plastic 1 and Plastic 2 are pneumatic plastic tubing from Festo, swaged with a $\frac{1}{4}$" brass ferrule. Plastic one connects a vacuum pump and the $\frac{1}{16}$" 3 point from Swagelok. Plastic 2 connects a vacuum pump (Pfeiffer DUO 3 M) the back pressure regulator(Bronkhorst El Press @Digital). The capillaries are described by their inner diameter ID, outer diameter OD and length L. Cap 1: $ID = 40\mu m$, $OD = 150\mu m$, $L = 41cm$. Cap 2: $ID = 100\mu m$, $OD = 238\mu m$, $L = 260cm$. Cap 3: $ID = 200\mu m$, $OD = 350\mu m$, $L = 39.5cm$. Cap 4: $ID = 150\mu m$, $OD = 363\mu m$, $L = 190cm$. Cap 5: $ID = 100\mu m$, $OD = 238\mu m$, $L = 114cm$. The sample gas was contained in a spherical gas container with a diameter of approximately 22 cm. The nafion was connected to the sample by being inserted in 2 large capillaries with $ID \approx 500\mu m$ and $L = 15cm$. The Carbon dioxide trap, Steel 2 was submerged in a $3l$ dewar(KGW isotherm). The combined flow control and flow meter was a MASS-FLO CONTROLLER from mks, controlled by a type 246 Pwr supply readout from mks. The Flow controller (Porter flow controller, model VCD 1000) has a range of $\approx 0 - 60 \frac{ml}{min}$. The flow meter was a Flow Tracker 1000 from Agilent. The oven was custom built, see section 2.11.1. Two different quartz tubes were used as reactor tubes for the oven, both of $L = 25cm$ the first with $OD = \frac{3}{8}$", the second with $OD = \frac{1}{4}$", the membrane was a perovskite membrane.

2.11.1 Building the Oven

For the previous measurement campaign, a larger oven was used [17]. It was $33cm$ long and had a diameter of $21cm$. It produced a power of approximately $220W$. The reactor quartz tubing going through had a large strain on the ends, which unfortunately caused that the quartz tube was broken when trying to make the old oven work. Due to this and that the length of the perovskite membrane did not need to be very long $5-10cm$, it was decided to create a new design with a more compact oven. This allowed for easier visual inspection of the membrane. Previously, the membrane was attached between two steel tubes [17]. A smaller reactor quartz tube would also benefit from needing less helium to transport the oxygen away. The oven setup was built upon Bianca Xuan Nguyen Larsen project [34], and the metal framework was also from her project. A sketch of the oven can be seen in figure 2.11.

The heating element of the oven was a thermocoax wire with a heating core, which was insulated with highly compacted mineral powder and had another metal layer around the powder, causing the wire to be electrically insulated. The heating wire was coiled around a quartz tube of length $15cm$, inner diameter $12mm$ and outer diameter $13mm$. Quartz glass was chosen due to its high resistance to temperature with a melting temperature at $1650°C$. The wire was coiled as close as possible around the tube and locked in place at the ends with duct tape.

While held in place, a high-temperature chemical cement (OMEGABOND OB-600) was prepared and applied on top of the heating wire. The cement powder was mixed with purified water with a ratio of 100 parts cement per 13 parts of water. This was measured with a high precision scale. Approximately $40g$ of the chemical cement powder was used. All water should applied simultaneously. Mixing of the cement was done with a cotton swab with the cotton part cut off. The mixed cement was liquid for approximately thirty minutes, after which a hardening process of approximately twenty-four hours was initialized.

The quartz tube was placed between two wood pieces where the cement could be applied, and the quartz was manually turned. Since the cement was liquid, the quartz tube had to be continually rotated every minute or so, to avoid gravity pulling the liquid down. After one hour, the quartz tube began to harden, and was placed in an oven set to $150°C$ for four hours. After four hours of baking, the cement was air-dried for twenty-four hours.

Several of the tube were prepared without the oven drying. This resulted in the cement cracking and starting to crumble in several places. With the chemical cement two ceramic pieces were attached to the hole in the circular metal sheets that the heating quartz tube were placed through. The purpose was to avoid having the quartz glass rest on the metal. In one end, the circular metal plate was removed, and the heating quartz tube was carefully inserted. On the wires, "ceramic pearls" were placed to provide heat insulation and protection from accidentally touching the wire.

While filling the oven with treated vermiculite mineral, the wires were pulled out through a small hole (in the circular metal sheets) and connected to a square ceramics connector. A DC power supply (Skytronic $0-60V$) was also connected the square ceramics connector

powering the heating wire. The circular metal sheet was re-attached, and a ground wire was connected to a flat head screw keeping the metal sheet in place.

The final wire had a resistance of 26 Ω. From Ohm's law, equation 2.19 and joule's first law, the power P in watt $[W]$, can be calculated:

$$P = I^2 R \tag{2.39}$$

where I is the current and R is the resistance. With $60V$ from the power supply, the oven has a power of $138W$ and produced a temperature of approximately $800°C$. The length of the heating wire was $2.08m$ allowing for a maximum power from the thermocoax of $208W$. This was due to the fact that the maximum power allowed in the thermocoax wire was $100\frac{W}{m}$. This allows for a higher temperature to be reached with a different power supply. Jesper Baldtzer Liisberg used a PID from Omega to control the temperature. With a PID, a fixed temperature setpoint can be selected with a chosen rate of temperature increase. This was tested for this setup as well, but for the measurements the temperature was controlled by the power supply.

Heating or cooling the oven was done in several voltage increments of approximately $10V$ per increment. This was to prevent damage on the wire, the membrane or the quartz tubing. The reactor quartz tube was held in place by a labstand and a small platform with adjustable height. At $800°C$, the oven was too hot to touch for more than a few seconds.

2.11.2 The Perovskite membrane

The perovskite membrane begins to transport oxygen through a partial pressure difference at approximately $600°C$. The Perovskite membrane was very fragile and must be handled with gloves. The membrane was sealed with a gold paste. The gold paste was applied with the plastic of a cotton swab and cured in an oven for 20 minutes at approximately $120°C$. The curing process removed some of the water of the gold paste. This process was repeated three to four times until a satisfactory seal was formed. Next the cured gold paste was placed in the oven and heated from room temperature to $800°C$ for an hour.

Jesper Baldtzer Liisberg cured the gold paste for three hours at $500°C$ [17], and Bianca Xuan Nguyen Larsen cured the gold paste for one hour at $500°C$ followed by $900°C$ [34] three hours. No evidence was found that the gold paste needed prolonged exposure to $950°C$ to work properly. The most crucial step was the initial curing at $120°C$.

The two capillaries going inside the membrane had their coating removed to prevent it from melting inside the membrane. The polyimide coating has a melting point of $400°C$. First, the capillaries were pushed through the double holed ferrule, and the correct length of the final capillary positions inside the membrane were noted. The coating was removed with a lighter. Without the coating, the capillary was more fragile. The two capillaries were placed inside the membrane by hand, and the membrane was placed inside the reactor quartz tube. This was rather tricky so a cotton swab was used to block one end to keep the membrane from going all the way through.

With the membrane placed in the middle of the heating zone of the oven, the capillaries were adjusted to their correction position while simultaneously sealing the reactor quartz tube with an Ultra-Torr fitting and Swagelok nut.
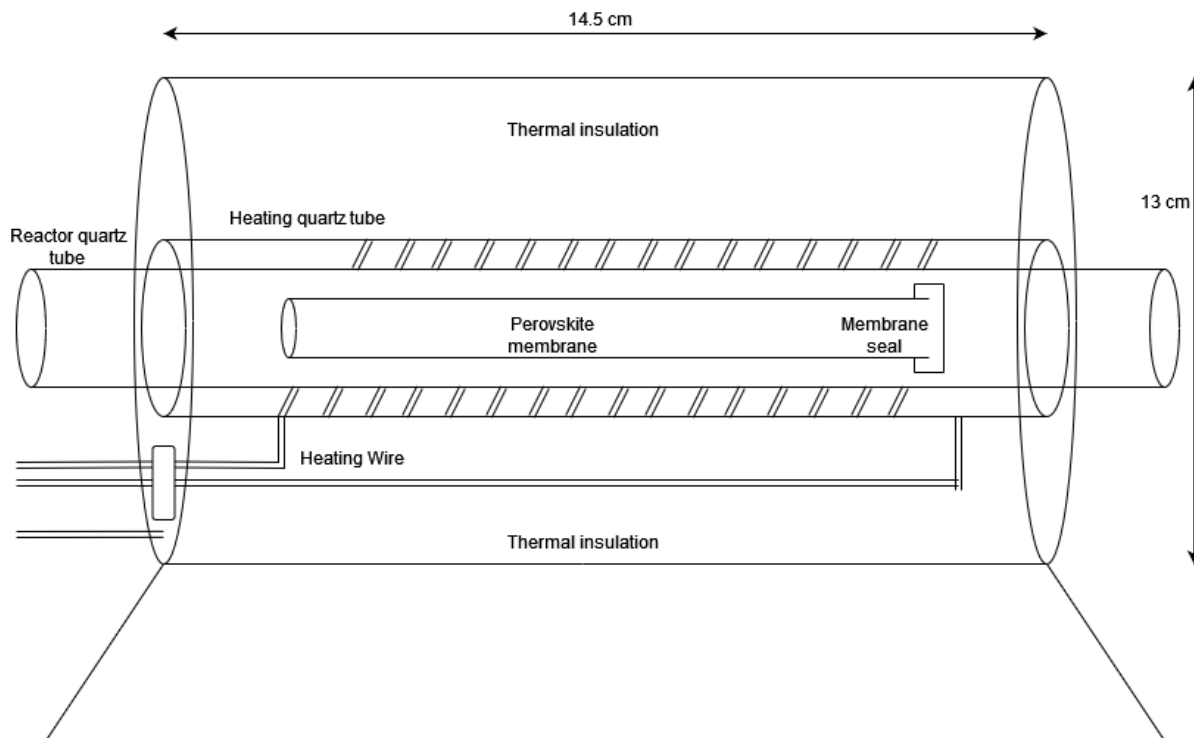
Figure 2.11: An illustration of the oven used for removing oxygen from the sample line. The framework is made of metal and consists of 2 parts, a cylindrical piece on top of a trapezoidal prism. A circular hole is in the middle of the circular metal sheets of the cylinder, through it the quartz tube with the heating wire rests on ceramic pieces. The heating wire was 1Ncl10 Heizleitermaterial from Thermocoax. The heating wire had an outer diameter of 1 mm, line resistance of $12.5\frac{\Omega}{m}$, maximum voltage of $110V$ and maximum power of $100\frac{W}{m}$. The heating quartz tube had a length of $15cm$. The reactor quartz tube had a length of $25cm$ and was held in place inside the heating quartz tube. The perovskite membrane was lying inside the reactor quartz tube and was sealed with gold paste (C 5754 B Conductor Paste from Heraeus. The oven was thermally insulated with vermiculite.

Chapter 3

Results

In this Chapter my results are presented. This includes results from the oven temperature, the mass signal intensities, the intensity ratios (isotopic and elemental), the zero enrichment measurement, the pressure imbalance measurements, the chemical slope measurements, the carbon dioxide removal, the oxygen removal efficiency and measurements of the final $\delta^{15}N$ and $\delta^{40}Ar$ values both with and without corrections.

3.1   Oven

While trying to find the correct resistance wire to use as a heating element for the oven, several different wires were tested. The different wires had different lengths and resistances and thus needs different power for the heating. The power presented is the power input of the total wire. The zone where the membrane and the thermocouple were located only received heating from the wire in the coils, wrapped around a quartz glass tube (heating tube). Hence the power to temperature relation is dependent on how much of the total wire length is in the coils.

The temperature was measured with a k-type thermocouple, the thermocouple was highly sensitive to its location in the oven. A displacement of a approximately $0.5cm$ in the hottest zone would change the temperature measured by approximately $5°C$. It should be noted that since the thermocouple was located between the heating tube and the reactor tube, the measured temperature would be smaller, than the temperature of the quartz tube, but larger than the temperature of the gas inside the membrane.

The power input was calculated with equation 2.19 and 2.39. While testing the different wires I measured their resistance using a multimeter and calculated the power from the applied voltage. The temperature was also observed, this can be seen in figure 3.1. The wire that ended up in the setup from figure 2.10 and 2.9 was the thermocoax wire, it had a length of $L = 2.08m$ with a resistance of 26Ω. The maximum operating power was $208W$ which would be achieved with voltage of $73.5V$.
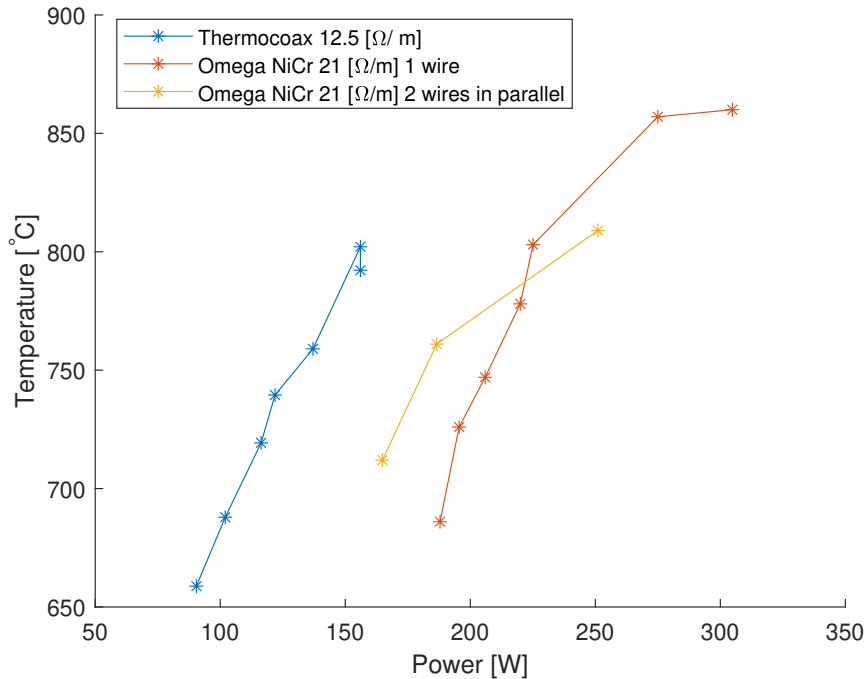
Figure 3.1: Measured temperature against supplied power for different heating wires. The blue stars are the thermocoax wire used in the final oven setup, the last point has the same power but a temperature difference of approximately $10°C$, this shows how sensitive the measured temperature was according to a slightly change of the location of the thermocouple. The red dots are from a single nickel chromium wire and the yellow dots are from a nickel chromium wire twisted around itself to let the current run in parallel.

3.2 Raw signal

When gas flows into the mass spectrometer the signal intensities can be read directly from the Isodat Instrument Control, the values are updated according to the chosen integration time (which was set to 1s). Numerous time scans were made were the mass intensities were recorded while testing the flow and tweaking different parameters e.g. the pressure regulators, the helium flow. This allowed for visual inspection of the effect of parameter tweaking and was generally helpful with the detection of problems. The visual inspection was also used to locate data that had to be removed for the manual calculation of the δ values, e.g. the spikes in the ratios of figure 3.3.

While measuring data for the pressure imbalance, the sample and reference inlet was switched, so a cut off point had to be defined to exclude data being measured, while the ion source was reaching a stable pressure. This corresponds to the idle time from Isodat Acquisition settings. The idle time was chosen roughly based in on this method. The "cut off" section was chosen based on the visual inspection of the raw ratios. An example of the measured signal intensities and the calculated signal ratios can be seen in figure 3.2 and 3.3.
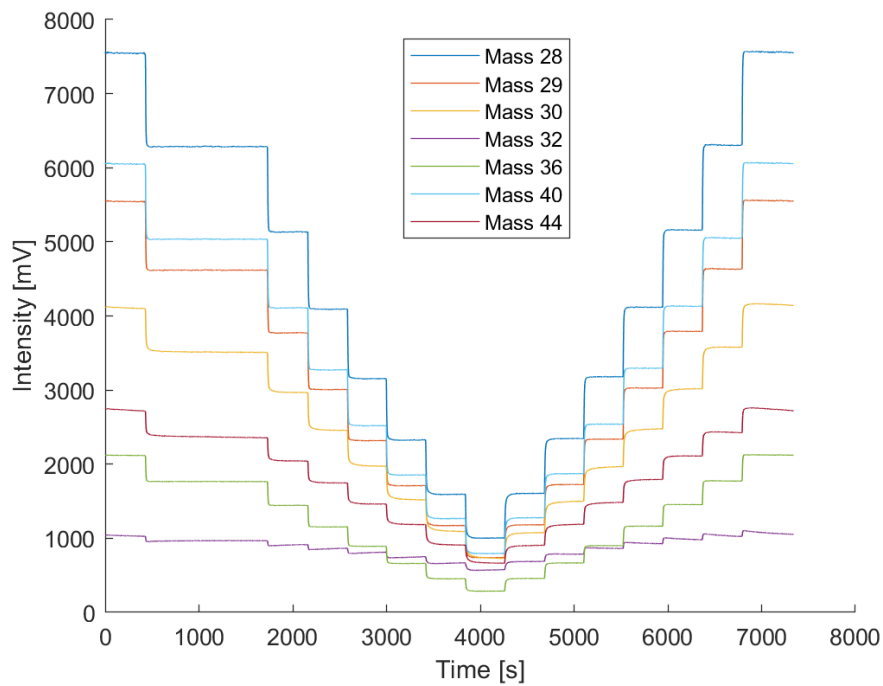
Figure 3.2: Mass intensities over time measured with Isodat Instrument Control time scan. The scan was done with the setup from figure 2.8. The data was only measured on the reference side. During the scan the pressure in the forward pressure regulators was changed from 110 to 40 to 110 *mbar* in steps of 10 *mbar*. Every data set corresponds to a mass being measured in the mass spectrometer. The measured masses are 28, 29, 30, 32, 36, 40 and 44. The measurement was done with the mixed nitrogen and argon standard.
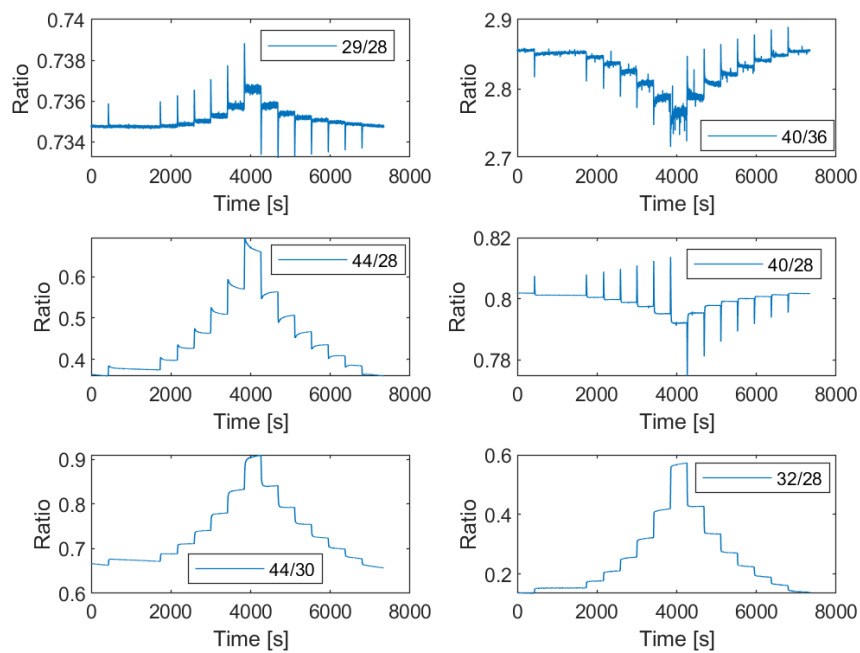
Figure 3.3: Time against the isotope and elemental ratios. The ratios are calculated based on the mass signal intensities from figure 3.2. Each subplot corresponds to a calculation of a ratio. The ratios measured are 29/28, 40/36, 44/28, 40/28, 44/30, 32/28. The spikes in the data corresponds to the pressure changes. It took some time until data stability was reached after a pressure change. The spikes and a certain amount of data after them was cut out of the data set before further calculations were done.

3.3   zero enrichment measurement

A zero enrichment measurement were done with isodat acquisition. The measurement was done with the setup from figure 2.8. The obtained $\delta^{15}N$ and $\delta^{40}Ar$ values with their respective uncertainty and standard error can be seen in table 3.1.

	δ value	Standard deviation	Standard error
$\delta^{15}N$	-0.0460 ‰	0.0120 ‰	0.0030 ‰
$\delta^{40}Ar$	-0.1220 ‰	0.1790 ‰	0.0450 ‰

Table 3.1: Zero enrichment test were done with Isodat Acquisition, the standard mixture of nitrogen and argon were used. The setup was that of figure 2.8. Both the back pressure regulator and forward pressure regulator were set to $50mbar$ and the test was measured over 16 cycles with an idle time of 60 seconds.

3.4   Pressure imbalance measurement

To correct for the pressure imbalances in the mass spectrometer the pressure imbalance slopes for $\delta^{15}N$, $\delta^{40}Ar$ $\delta\frac{Ar}{N_2}$ were experimentally derived. The measured and calculated $\delta^{15}N$ and $\delta^{40}Ar$ are shown in figure 3.4 and the pressure imbalance slopes needed for pressure imbalance corrections are shown in figure 3.5, 3.6 and 3.7.

The pressure imbalance effect was measured with three different methods all based on the setup from figure 2.8. For all three the pressure set point was changed on the pressure regulator every 10 minutes, this changed the flow into the mass spectrometer and the measured signal intensities.

For the first method a time scan was used on flow into the sample inlet, the δ values were calculated from the mass intensities with a manually chosen reference level. The pressure regulator was changed from $110mbar$ to $20mbar$ back to $110mbar$, this is why there are duplicate measurements for the same intensity levels. For the second and third method the data was measured with Isodat Acquisition, each δ value corresponds to one acquisition run for a certain pressure difference between sample and reference site. With the second method (the stars) I manually calculated the δ values from the raw acquisition intensities. This was done to make sure my coding agreed with that of Isodat Acquisition. The third method (the circles) was to let Isodat Acquisition calculate the δ values. The acquisition runs were done with 7 cycles and an idle time of 120 seconds, the data was integrated over 8 seconds. Note that the manual scan data was done on a different day than the acquisition runs.

The pressure imbalance slopes were found from the linear fit of the relationship between the δ values and the mass intensities from figure 3.5, 3.6 and 3.7 and they were found to be $\alpha_{PI^{15}N} = 5.517 \cdot 10^{-5} \frac{‰}{mV}$, $\alpha_{PI^{40}Ar} = 0.4161 \cdot 10^{-3} \frac{‰}{mV}$ and $PI\alpha_{\frac{Ar}{N_2}} = 0.3584 \cdot 10^{-3} \frac{‰}{mV}$. They were calculated using the data of the second method.
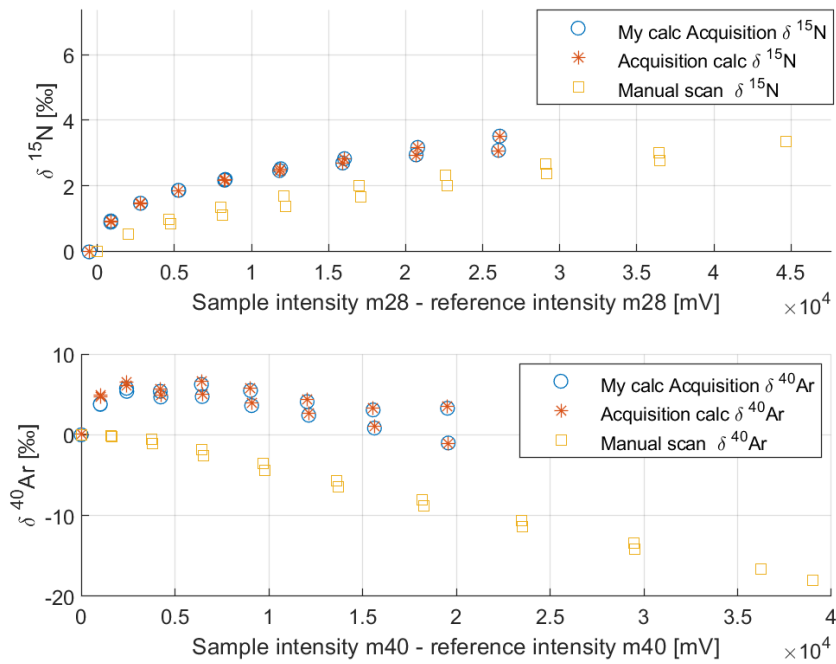
Figure 3.4: δ measurements of ^{15}N and ^{40}Ar vs the intensity difference between sample and reference of the dominant mass, 28 and 40. The δ values were calculated with three different methods. The circle data shows the δ calculated manually with the signal intensities obtained from Isodat Acquisition. The star data shows the δ values calculated by Isodat Acquisition. The squares shows the δ values where data was measured from a time scan of the sample inlet. The data was measured over 7 cycles with an idle time of 120 seconds, the data was integrated over 8 seconds. The reference intensity for mass 28 was approximately $2V$ for the manual scan and $1.9V$ for the acquisition data. The reference intensity for mass 40 was approximately $1.6V$ for the manual scan and $1.5V$ for the acquisition data.
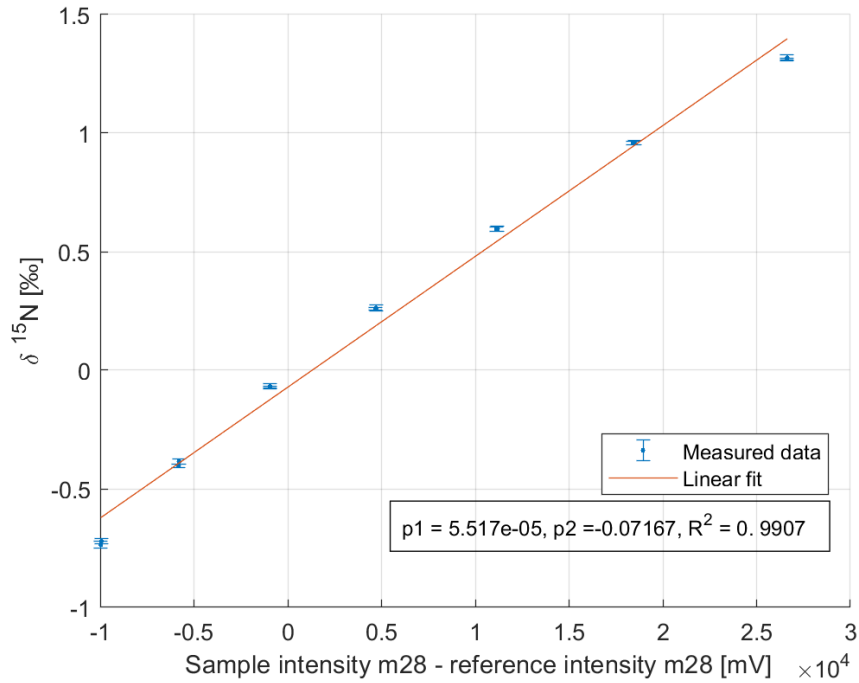
Figure 3.5: $\delta^{15}N$ vs the difference between the sample and reference intensity of mass 28. The blue dots are δ values obtained from Isodat Acquisition with their uncertainty obtained from the acquisition calculation. The red line is the linear fit made from a first order polynomial regression. From the fit the slope p1 $[\frac{‰}{mV}]$ and the interception p2 [‰] was found. Note that the data is not the same plotted in figure 3.4
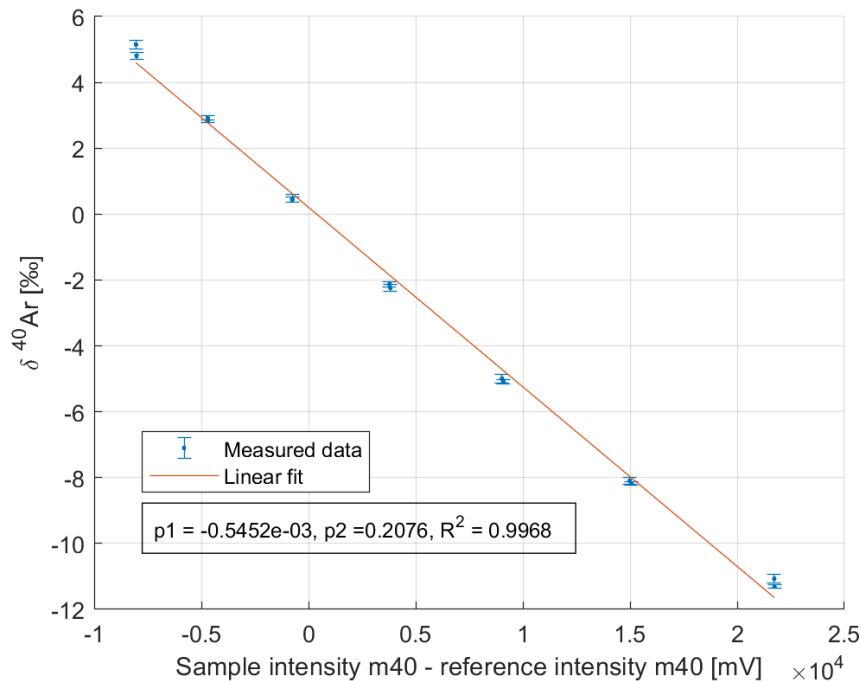
Figure 3.6: $\delta^{40}Ar$ vs the difference between the sample and reference intensity of mass 40. The blue dots are δ values obtained from Isodat Acquisition with their uncertainty obtained from the acquisition calculation. The red line is the linear fit made from a first order polynomial regression. From the fit the slope p1 $[\frac{‰}{mV}]$ and the interception p2 [‰] was found. Note that the data is not the same plotted in figure 3.4
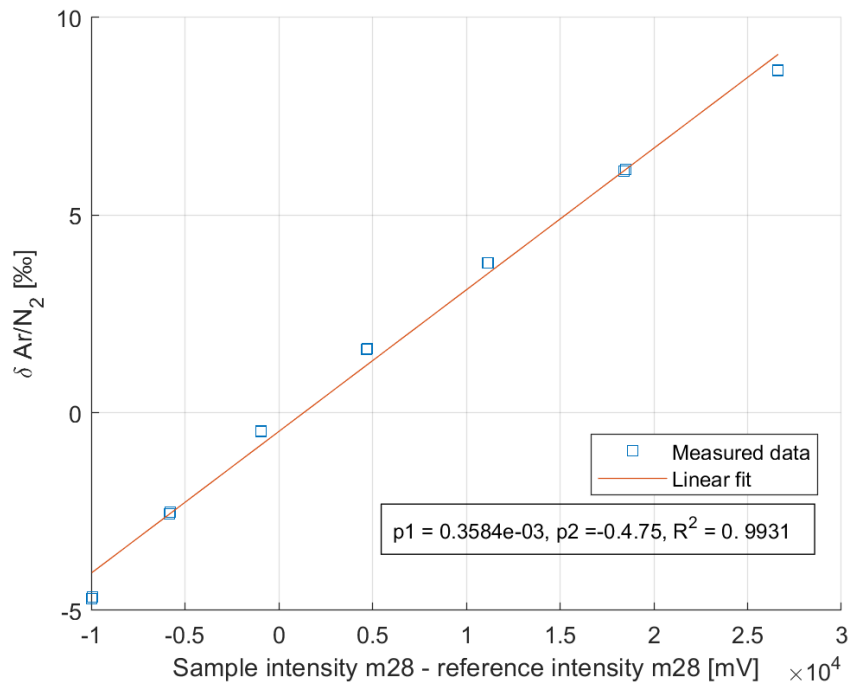
Figure 3.7: $\delta \frac{Ar}{N_2}$ vs the difference between the sample and reference intensity of mass 28. The blue dots are δ values obtained from Isodat Acquisition with their uncertainty obtained from the acquisition calculation. The red line is the linear fit made from a first order polynomial regression. From the fit the slope p1 $[\frac{‰}{mV}]$ and the interception p2 [‰] was found.

3.5   Chemical slope measurements

Small changes in the gas composition affects the measured δ values. To correct for this, a series of separate measurements were made where pure nitrogen, argon, oxygen and carbon dioxide were added to the gas flow into the sample inlet. Nitrogen was added to measure the effect on $\delta^{40}Ar$, argon was added to measure the effect $\delta^{15}N$. Oxygen and carbon dioxide was added to motivate the removal of these in the sample stream for the final measurements. All chemical slopes were found with the setup from figure 2.8 and has been corrected for the pressure imbalance.

The nitrogen and argon chemical slopes were found with the acquisition with a constant flow of gas into the mass spectrometer. The slope was found by changing the pressure regulator on the nitrogen or argon bottle from 3 bar to 1.2 bar. Different capillaries were used to mix the added gas into the sample streams.

From figure 3.8, it can be seen that, $\delta^{15}N$ changed by about 0.04 ‰ when $\delta\frac{Ar}{N_2}$ increased by almost 600 ‰. From figure 3.9, it can be seen that, $\delta^{40}Ar$ changed by about 25 ‰ when $\delta\frac{Ar}{N_2}$ increased by about 350 ‰. The chemical slopes for nitrogen and argon were found with a linear fit as can be seen in figure 3.8 and 3.9. They were found to be: $\alpha_{CS\delta15N} = 7.176 \cdot 10^{-6}$ and $\alpha_{CS\delta40Ar} = 0.07579$.

For the oxygen and carbon dioxide slopes a small volume was filled and and mixed gradually into the sample air stream as the pressure in the volume drops over time. The data was measured with a mass intensity vs time scan. A reference level was first measured for 10 minutes, then the added gas was released and the δ values were calculated as volume emptied over time. The effect on the δ values from introducing oxygen into the sample stream can be seen in figure 3.10, 3.11 and 3.12. The effect on the δ values from introducing carbon dioxide into the sample stream can be seen in figure 3.13, 3.14 and 3.15. Before oxygen and carbon dioxide was released a reference level was measured over 10 minutes. From a time perspective the δ values were initially 0, then they became relatively large with the initial burst of introduced gas before slowly going back to the pre-introduction level. The δ values should be read from most left ($\delta = 0$) jump all the way to the right and then changing towards the left. Note that $\delta\frac{Ar}{N_2}$ behaves non-linearly.
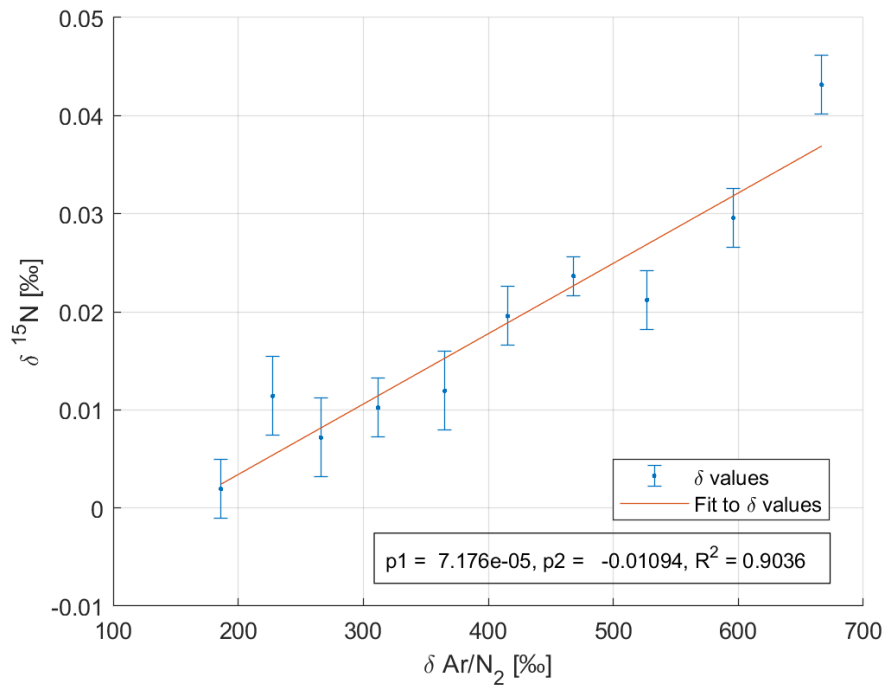
Figure 3.8: $\delta^{15}N$ vs $\delta\frac{Ar}{N_2}$. The blue dots are the data measured and the red line is the linear fit made by from a first order polynomial regression to the data. The measurement were conducted by changing the pressure regulator on the argon bottle from 3 bar to 1.2 in steps of 0.2 bar. The data uncertainties ware calculated by Isodat Acquisition. From the linear regression the slope p1 and the interception p2 [‰] was calculated.
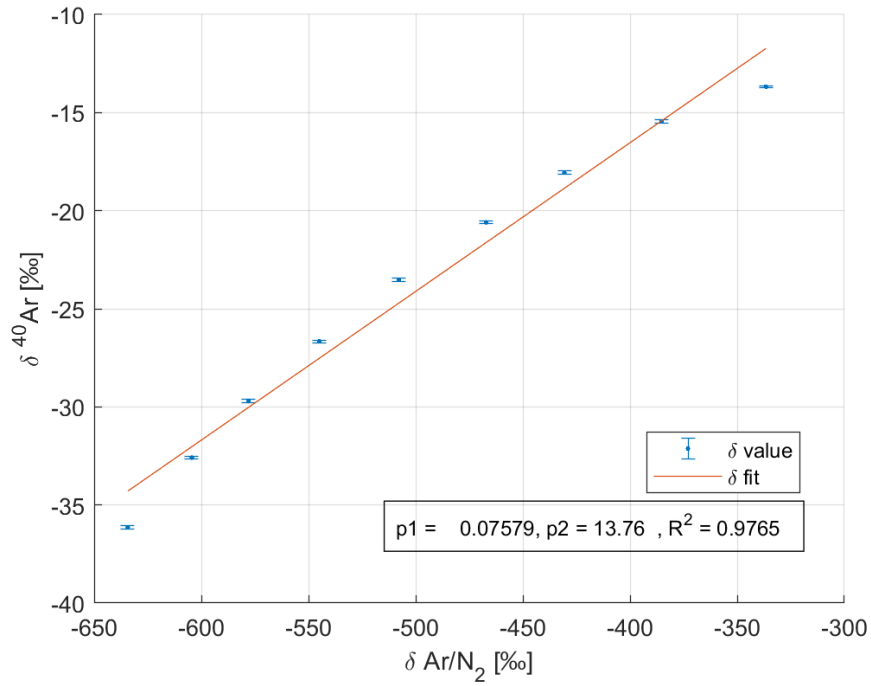
Figure 3.9: $\delta^{40}N$ vs $\delta\frac{Ar}{N_2}$. The blue dots are the data measured and the red line is the linear fit made by from a first order polynomial regression to the to the data. The data was obtained using Isodat Acquisition while changing the pressure regulator on the nitrogen bottle from 3 bar to 1.2 in steps of 0.2 bar. The data uncertainties ware calculated by Isodat Acquisition. From the linear regression the slope p1 and the interception p2 [‰] was calculated.
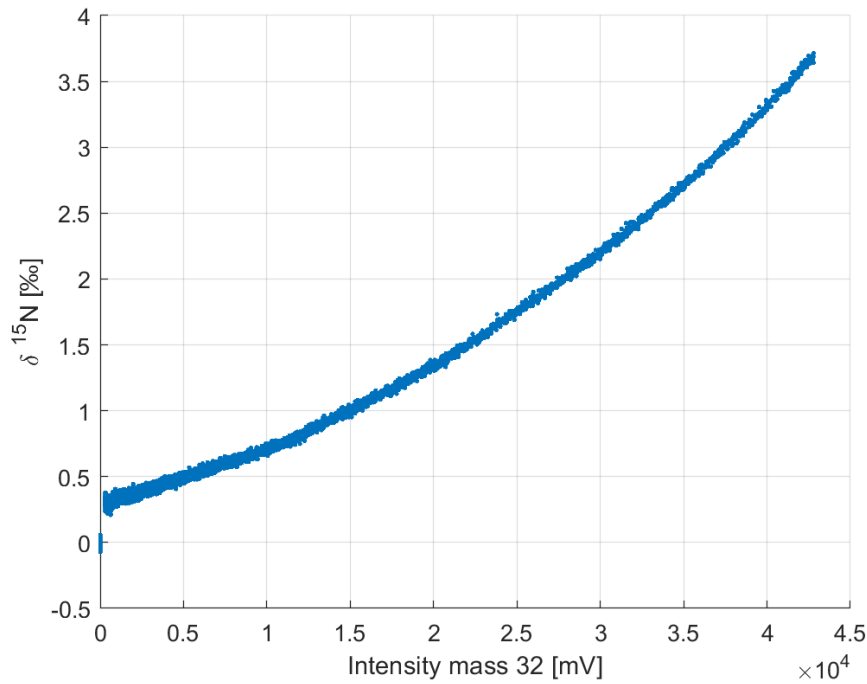
Figure 3.10: $\delta^{15}N$ vs intensity of mass 32. The dots are the calculated data from a manual intensity vs time scan. The change in the δ values were found by measuring a reference level then releasing all oxygen from a volume at a gradual decrease over time.
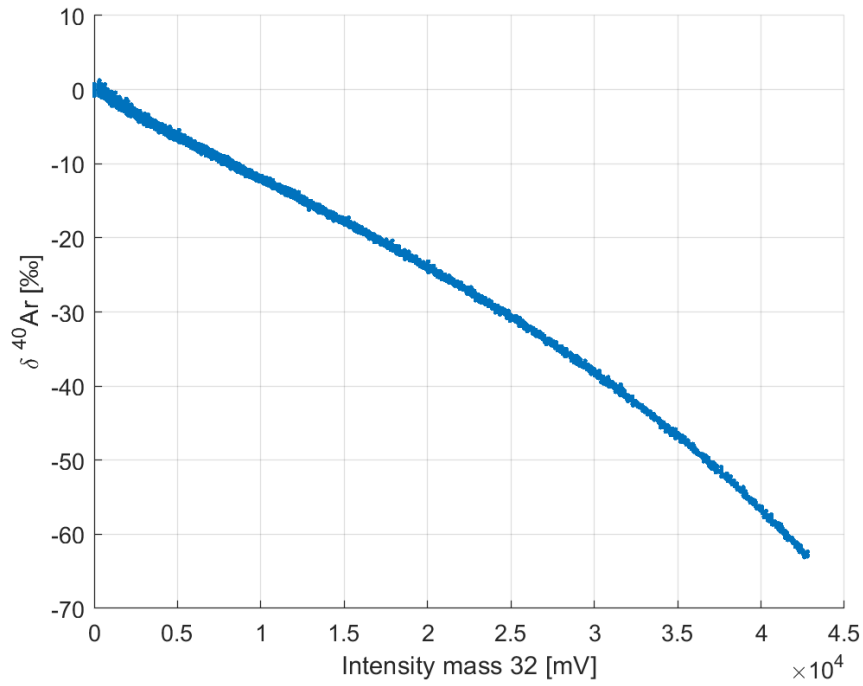
Figure 3.11: $\delta^{40}Ar$ vs intensity of mass 32. The dots are the calculated data from a manual intensity vs time scan. The change in the δ values were found by measuring a reference level then releasing all oxygen from a volume at a gradual decrease over time.
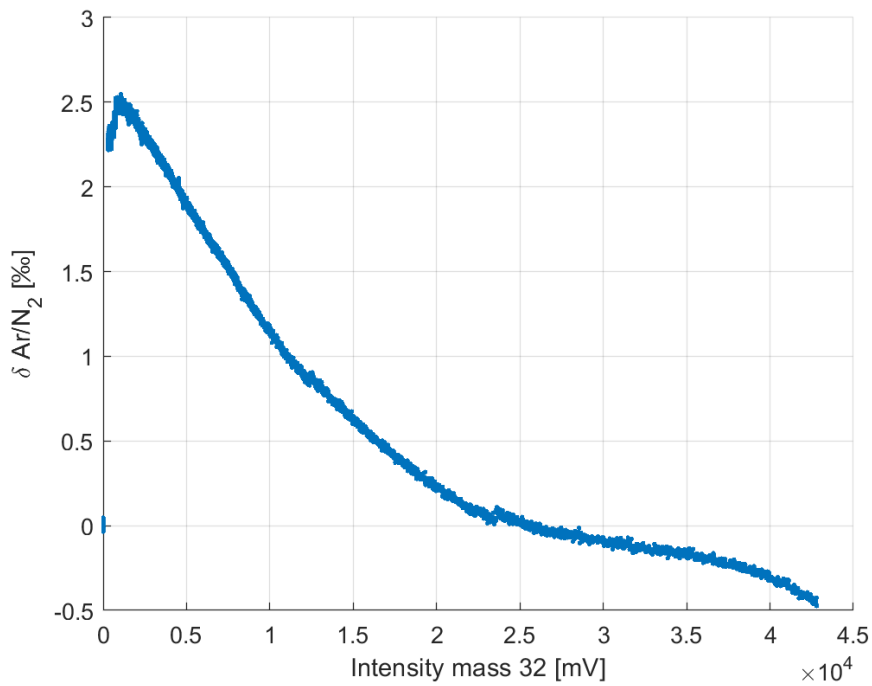
Figure 3.12: $\delta\frac{Ar}{N_2}$ vs intensity of mass 32. The dots are the calculated data from a manual intensity vs time scan. The change in the δ values were found by measuring a reference level then releasing all oxygen from a volume at a gradual decrease over time.
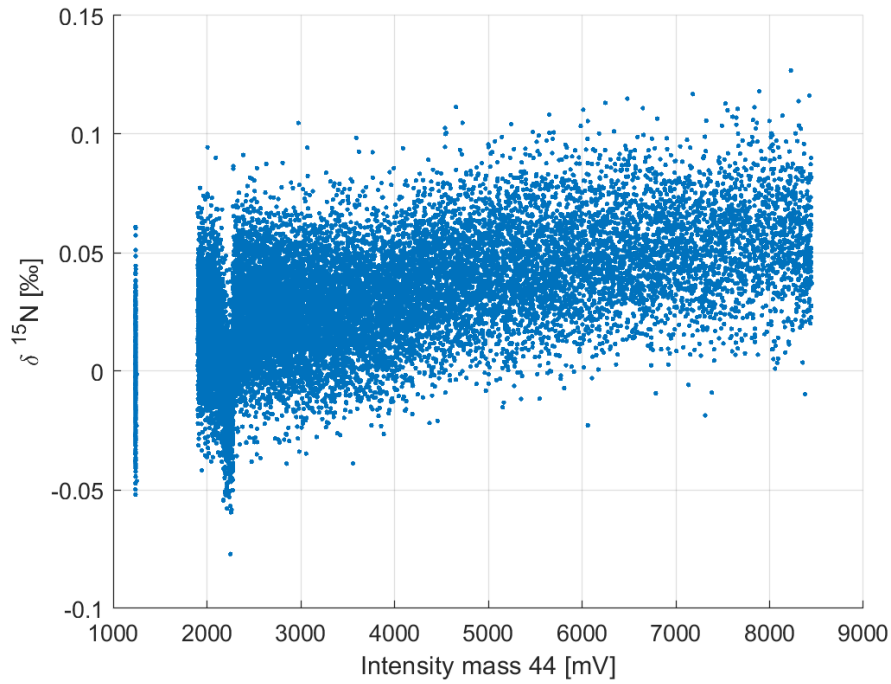
Figure 3.13: $\delta^{15}N$ vs intensity of mass 44. The dots are the calculated data from a manual intensity vs time scan. The change in the δ values were found by measuring a reference level then releasing all Carbon dioxide from a volume at a gradual decrease over time.
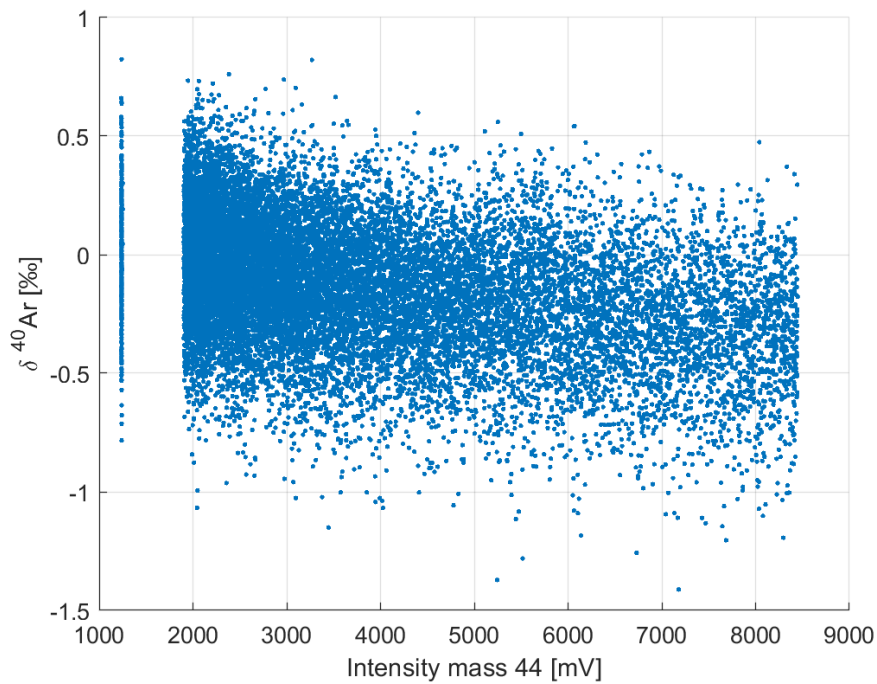
Figure 3.14: $\delta^{40}Ar$ vs intensity of mass 44. The dots are the calculated data from a manual intensity vs time scan. The change in the δ values were found by measuring a reference level then releasing all Carbon dioxide from a volume at a gradual decrease over time.
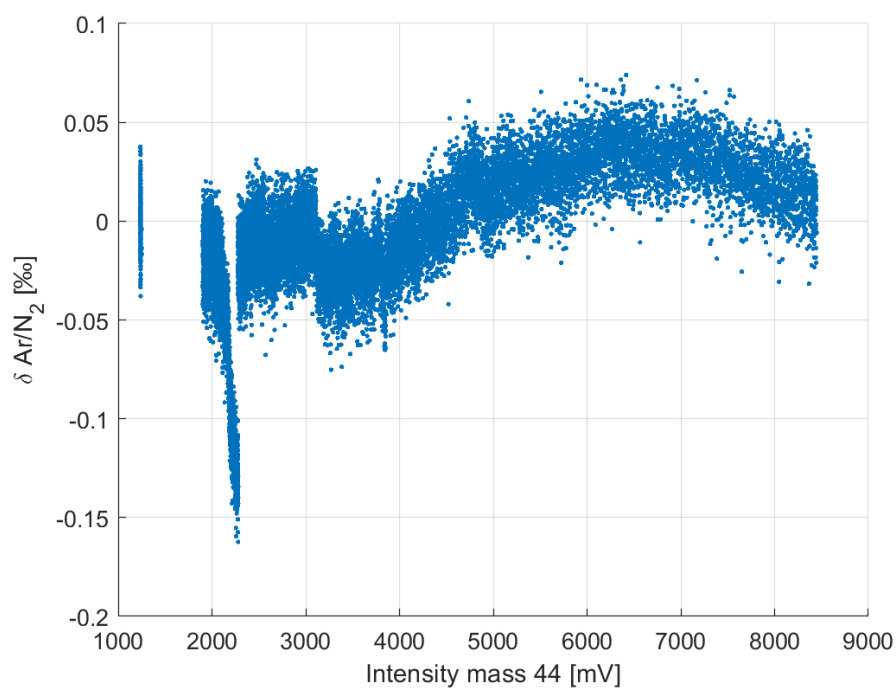
Figure 3.15: $\delta \frac{Ar}{N_2}$ vs intensity of mass 44. The dots are the calculated data from a manual intensity vs time scan. The change in the δ values were found by measuring a reference level then releasing all Carbon dioxide from a volume at a gradual decrease over time.

3.6 Carbon dioxide removal and oven effect on oxygen

Carbon dioxide was removed from the sample stream with a liquid nitrogen trap. An intensity vs time scan can be seen in figure 3.16, the scan was made with the setup from figure 2.10 and 2.9. The figure shows the measured intensities of mass 28, 32 and 44. The effect of heating the oven on measurement values can be seen as all masses decreases, this is because the flow into the mass spectrometer is constant but the gas expands and therefor has a lower density. At temperatures at approximately $600°C$, the membrane is activated and oxygen is removed from the sample stream, hence the intensity of mass 32 drops very fast to a low level. The effect on mass 44 adding liquid nitrogen into the CO_2 trap can be seen as the intensity rapidly drops. There is also a quick drop in all the other masses as can be seen on mass 28, this happens because the volume of the gas (and thus the pressure) in the steel tube of the trap gets smaller due to the fast cooling and it takes a second for the gas to reach equilibrium again.
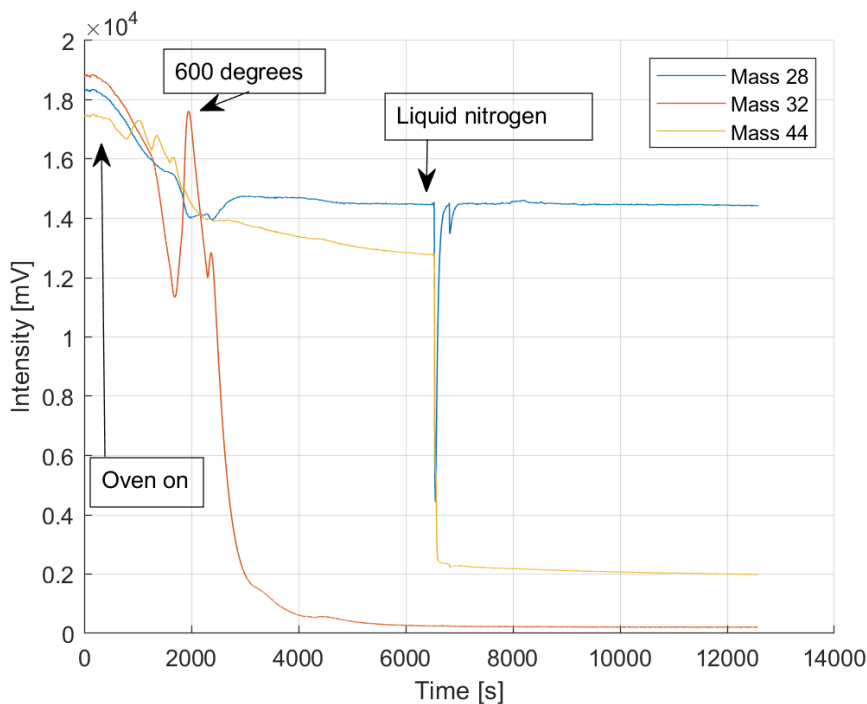
Figure 3.16: Time vs intensity scan. The blue data is mass 28, the red data is mass 32 and the yellow data is mass 44. The scan was started after the flow had been running for some time and was in equilibrium. The oven is turned on first after 10 minutes of scan, this affected all the masses, after the oven has reached approximately $600°C$ the membrane activates and the intensity of mass 32 is reduced to approximately $200mV$. At approximately 6500 seconds liquid nitrogen was added to the dewar and the intensity of mass 44 was reduced to approximately $2000mV$.

3.7 Oxygen removal measurements

Oxygen was removed from the sample stream with a perovskite membrane, and the removal efficiency was determined. The ratio between between oxygen and nitrogen intensities can be seen in figure 3.17. The sample stream was allowed to flow for approximately two hours, then a scan of the intensities of oxygen and nitrogen was measured for two minutes. The oxygen and nitrogen ratio could be calculated and the mean value of two minute scan were used for determining the oxygen removal efficiency. The oxygen removal rate dependency on temperature can be seen in figure 3.18 and the oxygen removal rate dependency on the helium stream can be seen in figure 3.19. The setup used was that of figure 2.10 and 2.9 and the liquid nitrogen trap was filled with liquid nitrogen for both measurements. In figure 3.18 a time scan was done of the intensity and the oxygen removal rate was calculated. The temperature was changed in approximately $20°C$ steps (arrows in figure 3.18 from highest temperature to lowest temperature. When lowering the temperature, it was found that the oxygen removal efficiency initially increased but lowered in time. The opposite was observed when increasing the temperature while testing. It was observed that it took approximately 4000 seconds for the removal efficiency to become stable after a temperature change. In figure 3.19 a time scan was done of the mass intensities and the oxygen removal rate was calculated. Here, the helium stream carrying the oxygen from the outside of the membrane to the pump was reduced, from $80\frac{ml}{min}$ in steps of $10\frac{ml}{min}$ and from $10\frac{ml}{min}$ in steps of $2\frac{ml}{min}$. The sample air flow into the membrane was in the order of $0.1\frac{ml}{min}$ and for the $\frac{5}{8}$" quartz tube the helium flow was 500 times bigger (than the sample flow) to achieve 99% removal rate.

3.7.1 Reconstruction of the oxygen signal

To calculate the removal rate of oxygen from the air sample, the measured signal on mass 32 was compared to the mass 32 signal which would have been measured if the oven was off. Therefor the signal on mass 32 had to be reconstructed. It was assumed that all the removed oxygen would be replaced by nitrogen in the sample stream. The new abundance of nitrogen in the oxygen depleted gas would be 0.9903 assuming no change in the argon concentration.

A measurement of the oxygen and nitrogen ratio without the oven but with the liquid nitrogen trap was done, and can be seen in 3.17. The mean value was calculated to be $1.0001 \pm 6.5499 \cdot 10^{-5}$. The mass 28 signal with the oxygen removal was larger than the mass 28 signal without heating the oven. To reconstruct the mass 28 level with the oven if oxygen would still be in the sample stream, the ratio between the real atmospheric nitrogen concentration and the enriched nitrogen concentration was calculated: $\frac{0.9903}{0.7815} = 0.7732$. The reconstructed mass 32 signal could now be found by $m32_{recreated} = mass28_{measured} \cdot 0.7732 \cdot 1.0001$. The ratio between the measured mass 32 and the reconstructed mass 32 was used to find the oxygen removal efficiency: Removal rate of $O_2 = (1 - \frac{mass32_{measured}}{mass32_{reconstructed}}) \cdot 100\%$.
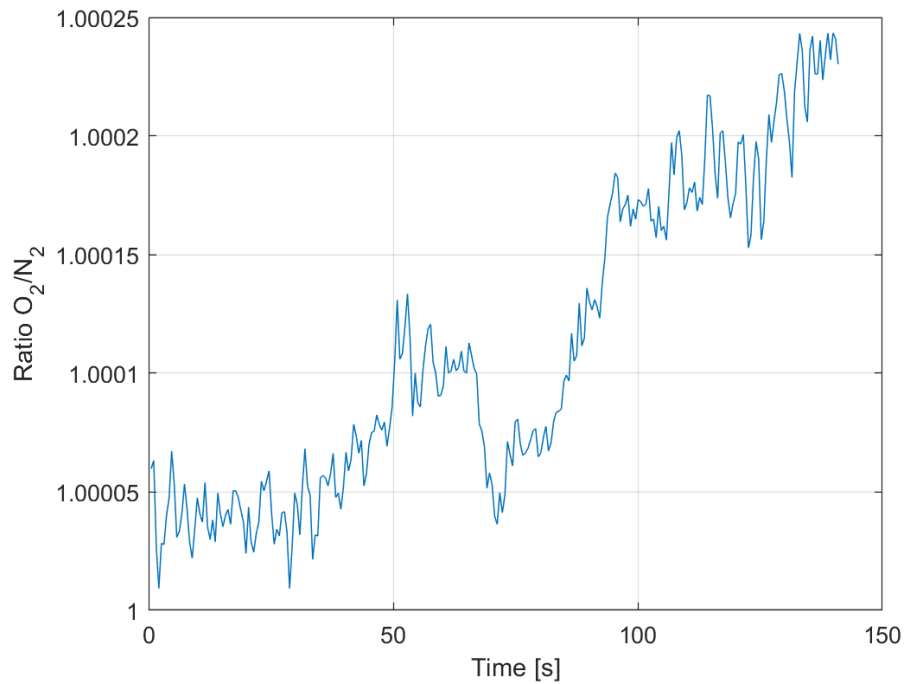
Figure 3.17: The ratio between oxygen and nitrogen vs time. The ratio was calculated based on the mass intensities 32 and 28. The final setup was used without heating the oven, but with the liquid nitrogen trap filled with liquid nitrogen.
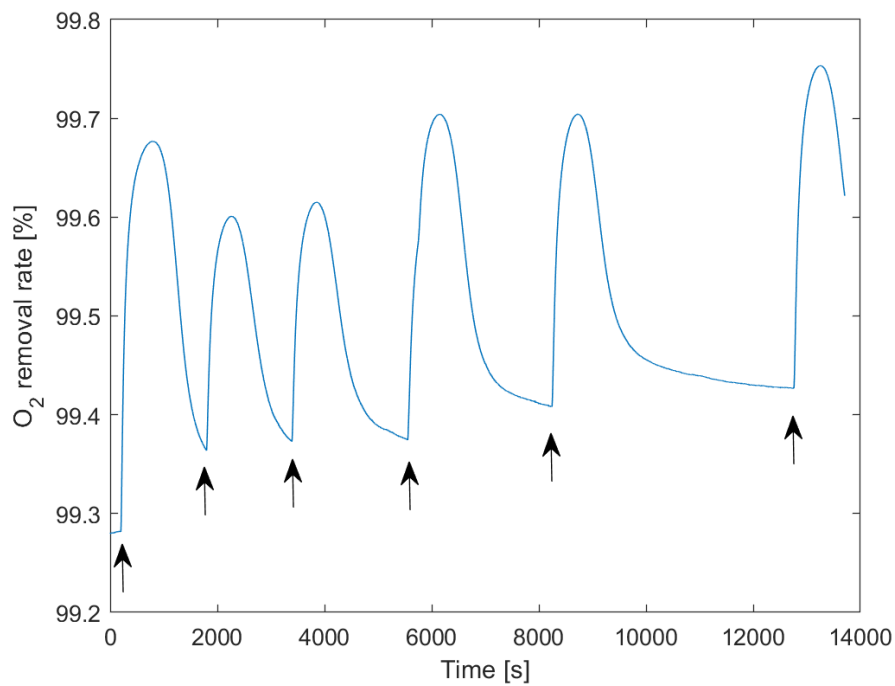
Figure 3.18: The removal rate of oxygen vs time. The temperature was changed where the arrows are placed, and from left to right: $790.0°C$, $759.0°C$ $739.5°C$, $719.3°C$, $687.9°C$ and $658.8°C$. The helium stream was constant at $80\frac{ml}{min}$ and the liquid nitrogen trap was filled with liquid nitrogen.
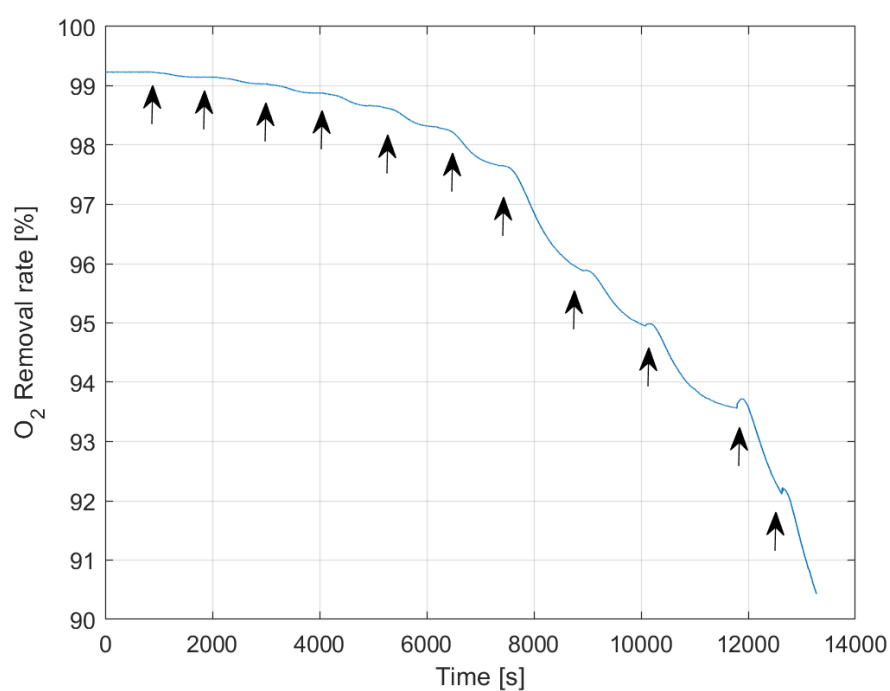
Figure 3.19: The removal rate of oxygen vs time. The helium stream was changed where the arrows are placed, and from left to right: $80\frac{ml}{min}$, $70\frac{ml}{min}$, $60\frac{ml}{min}$, $50\frac{ml}{min}$, $40\frac{ml}{min}$, $30\frac{ml}{min}$, $20\frac{ml}{min}$, $10\frac{ml}{min}$, $8\frac{ml}{min}$, $6\frac{ml}{min}$, $4\frac{ml}{min}$. The temperature was constant at $798.5°C$ and the liquid nitrogen trap was filled with liquid nitrogen.

3.8 Final measurements with oxygen removal

With the liquid nitrogen trap and the oxygen removal active, four acquisition runs were done to measure $\delta^{15}N$ and $\delta^{40}Ar$ from NEEM air. The measured δ values, the standard deviation and standard error can be seen in table 3.2 and 3.3. The δ values corrected for the zero enrichment, the pressure imbalance and the chemical slope can be seen in table 3.4 and 3.5. For the corrected values the uncertainties have been error propagated with the equations from section 2.7.5. The differences between the acquisition runs (listed below) were used to test the stability and the precision of the setup when parameters were changed.

- Acquisition 1: Normal run.
  Helium flow of $80\frac{ml}{min}$, oven temperature at $758.9°C$, back pressure regulator set to $100mbar$, forward pressure regulator set to $37mbar$, 16 cycles and an integration time of 10 seconds

- Acquisition 2: Testing the effect of the integration time.
  helium flow of $80\frac{ml}{min}$, oven temperature at $758.9°C$, back pressure regulator set to $100mbar$, forward pressure regulator set to $37mbar$, 16 cycles and an integration time of 20 seconds

- Acquisition 3: Reducing oven temperature. Note that the sample flow with the forward pressure regulator had to be adjusted to match the changed mass intensities from a change in temperature.
  Helium flow of $80\frac{ml}{min}$, oven temperature at $621.0°C$, back pressure regulator set to $100mbar$, forward pressure regulator set to $41mbar$, 16 cycles and an integration time of 20 seconds.

- Acquisition 4: High flow difference between sample and reference side (mass 28: 40 V for reference, 2 V for sample).
  Helium flow of $80\frac{ml}{min}$, oven temperature at $788.2°C$, back pressure regulator set to $20mbar$, forward pressure regulator set to $100mbar$, 16 cycles and an integration time of 20 seconds.

Acquisition number	$\delta^{15}N_{raw}$ [‰]	Standard deviation $\delta^{15}N_{raw}$ [‰]	Standard error $\delta^{15}N_{raw}$ [‰]
1	4.782	0.0120	0.0030
2	4.780	0.0060	0.0010
3	4.648	0.0070	0.0020
4	2.315	0.0180	0.0040

Table 3.2: Table of the measured $\delta^{15}N_{raw}$, the standard deviation and the standard error. Four different acquisition measurements were conducted to test the stability of the setup. The setup was that of figure 2.10 and 2.9. The first acquisition was done with a helium flow of $80\frac{ml}{min}$, oven temperature at $758.9°C$, back pressure regulator set to $100mbar$, forward pressure regulator set to $37mbar$, 16 cycles and an integration time of 10 seconds. The only difference for second acquisition was that the integration time had been changed to 20 seconds. The third acquisition was done with a helium flow of $80\frac{ml}{min}$, oven temperature at $621.0°C$, back pressure regulator set to $100mbar$, forward pressure regulator set to $41mbar$, 16 cycles and an integration time of 20 seconds. The fourth acquisition run was done with a helium flow of $80\frac{ml}{min}$, oven temperature at $788.2°C$, back pressure regulator set to $20mbar$, forward pressure regulator set to $100mbar$, 16 cycles and an integration time of 20 seconds.

Acquisition number	$\delta^{40}Ar_{raw}$ [‰]	Standard deviation $\delta^{40}Ar_{raw}$ [‰]	Standard error $\delta^{40}Ar_{raw}$ [‰]
1	-2.069	0.1580	0.0400
2	-2.055	0.0990	0.0250
3	-1.762	0.0720	0.0180
4	-18.937	0.1940	0.0480

Table 3.3: Table of the measured $\delta^{40}Ar_{raw}$, the standard deviation and the standard error. Four different acquisition measurements were conducted to test the stability of the setup. The setup was that of figure 2.10 and 2.9. The first acquisition was done with a helium flow of $80\frac{ml}{min}$, oven temperature at $758.9°C$, back pressure regulator set to $100mbar$, forward pressure regulator set to $37mbar$, 16 cycles and an integration time of 10 seconds. The only difference for second acquisition was that the integration time had been changed to 20 seconds. The third acquisition was done with a helium flow of $80\frac{ml}{min}$, oven temperature at $621.0°C$, back pressure regulator set to $100mbar$, forward pressure regulator set to $41mbar$, 16 cycles and an integration time of 20 seconds. The fourth acquisition run was done with a helium flow of $80\frac{ml}{min}$, oven temperature at $788.2°C$, back pressure regulator set to $20mbar$, forward pressure regulator set to $100mbar$, 16 cycles and an integration time of 20 seconds.

Acquisition number	$\delta^{15}N_{corr}$ [‰]	Standard deviation $\delta^{15}N_{corr}$ [‰]
1	4.787	0.0120
2	4.785	0.0060
3	4.649	0.0070
4	4.503	0.0689

Table 3.4: Table of the measured $\delta^{15}N_{corr}$ corrected for the zero enrichment, pressure imbalance and chemical slope, the standard deviation and the standard error. Four different acquisition measurements were conducted to test the stability of the setup. The setup was that of figure 2.10 and 2.9. The first acquisition was done with a helium flow of $80\frac{ml}{min}$, oven temperature at $758.9°C$, back pressure regulator set to $100mbar$, forward pressure regulator set to $37mbar$, 16 cycles and an integration time of 10 seconds. The only difference for second acquisition was that the integration time had been changed to 20 seconds. The third acquisition was done with a helium flow of $80\frac{ml}{min}$, oven temperature at $621.0°C$, back pressure regulator set to $100mbar$, forward pressure regulator set to $41mbar$, 16 cycles and an integration time of 20 seconds. The fourth acquisition run was done with a helium flow of $80\frac{ml}{min}$, oven temperature at $788.2°C$, back pressure regulator set to $20mbar$, forward pressure regulator set to $100mbar$, 16 cycles and an integration time of 20 seconds.

Acquisition number	$\delta^{40}Ar_{corr}$ [‰]	Standard deviation $\delta^{40}Ar_{corr}$ [‰]
1	6.078	0.1581
2	6.064	0.0991
3	5.8465	0.0722
4	5.8519	0.3687

Table 3.5: Table of the measured $\delta^{40}Ar_{corr}$ corrected for the zero enrichment, pressure imbalance and chemical slope, the standard deviation and the standard error. Four different acquisition measurements were conducted to test the stability of the setup. The setup was that of figure 2.10 and 2.9. The first acquisition was done with a helium flow of $80\frac{ml}{min}$, oven temperature at $758.9°C$, back pressure regulator set to $100mbar$, forward pressure regulator set to $37mbar$, 16 cycles and an integration time of 10 seconds. The only difference for second acquisition was that the integration time had been changed to 20 seconds. The third acquisition was done with a helium flow of $80\frac{ml}{min}$, oven temperature at $621.0°C$, back pressure regulator set to $100mbar$, forward pressure regulator set to $41mbar$, 16 cycles and an integration time of 20 seconds. The fourth acquisition run was done with a helium flow of $80\frac{ml}{min}$, oven temperature at $788.2°C$, back pressure regulator set to $20mbar$, forward pressure regulator set to $100mbar$, 16 cycles and an integration time of 20 seconds.

Chapter 4

Discussion

4.1   Oven

One of the main objectives of this thesis was to create a more compact oven. This was achieved with a thermocoax wire, this setup only required $63.7V$ to achieve $156W$. For reference the larger oven ran with $220V$ AC, and consumed approximately $220W$. The smaller more compact oven had the advantage of having a smaller heat loss to the surroundings, but the disadvantage was, that a relatively longer part of the heating wire was placed outside of the hot zone. Further testing with a different power supply (because the power supply had max voltage output of $63.7V$) could be done to reach higher temperatures.

During the oven testing I used both a PID (proportional integral derivative) and the power supply to control the oven temperature. The PID turns the provided power supply on and off, every time the measured temperature is above or below a threshold determined from the set point. This caused the temperature to fluctuate with $\pm2°C$ around the set point. With the power supply manually controlled the temperature fluctuations where in the order of $\pm0.2°C$. The PID could control the rate of temperature change and it was easier to reach specific set points. A trade off between precision and control of the temperature was made and the precision was favored.

A problem with the different heating wires, available from the laboratory supply, was that the maximum current allowed, were too low relative to the voltage I wanted to supply. Therefor it was not possible to use the same wire as for the larger oven, it was physically impossible to get enough coils around the smaller and shorter quartz tube.

A thermocoax resistance wire with a larger maximum power per meter would be optimal. From figure 3.1 it can be seen that the thermocoax wire (blue stars) is the most efficient of the three investigated heating wires. The power was equal for the last two points of the thermocoax wire, this shows how tricky it was to locate the thermocouple. The thermocouple barely fitted in between the two quartz tubes, and had to bent in order to fit because of the Ultra-Torr connection at the end of the reactor quartz tube. The reason that the thermocoax wire was more efficient than the nickel chromium was because I was able to get more coils onto the quartz tube due to the fact that it had a lower resistance

per meter and was electrically insulated.

It should be noted that when turning off the power supply it takes approximately 2-3 hours before the oven is back to room temperature.

4.2 Raw signals

An example of time scan measurement with the mass signal intensities can be seen in figure 3.2 and the calculated elemental and isotopic ratios can be seen in figure 3.3. It was the standard made from mixed nitrogen and argon that was measured and the measurement was done quite early in the setup development.

When measuring a nitrogen and argon mixture it would be expected that mainly mass 28, 29, 36 and 40 would show signal intensities larger than a hundred mV. In the case of this measurement we have a significant signal on mass 32 of $1V$ and on mass 44 of $\approx 3to1V$ which means that a leak was present in the line. A series of steps were initiated in order to find and remove the leak. The first step was to blow on every Swagelok part to see if any was incorrectly tightened, blowing on the parts would dramatically increase the CO2 intensity due to the high concentration in a breath relative to atmospheric air. Second step was to spray the Swagelok parts with a capillary connected to an argon bottle, this would dramatically increase the argon signal. The third step was to make sure that the correct ferrule size were used in the capillary connections. The last step was to carefully slightly tighten the connections, this step is a last resort because of the probability to accidentally damaging the connections by over tightening.

During the course of my thesis a leak was virtually present every time the setup was changed. This was because I had to learn my way around the laboratory and some of the connections of the connections were previously used and partially damaged. This troubleshooting process eventually eliminated all leaks that arose.

When calculating the δ values only the stable part of a measurement was used, the data points immediately following a flow change, when switching between sample and reference inlet, or changing the pressure in the reactor tube, were removed. The data points to be removed were chosen manually, by visually inspecting when the ratios became stable.

4.3 Zero enrichment test

A zero enrichment test was done and the internal precision for $\delta^{15}N$ and $\delta^{40}Ar$ was found to be $-0.0460‰ \pm 0.003$ and $-0.1220‰ \pm 0.045$, respectively. Unfortunately the test was done 2 months prior to the final measurement. For a measurement campaign the zero enrichment measurement should be done on the same day as the measurement. For this option a slight change in the final setup needs to be included. To allow for the standard mixture to be measured on the sample side in the final setup from figure 2.10 and 2.9. This would be achieved by installing a three point valve at the sample inlet. This will also allow for pressure imbalance corrections and chemical slope corrections to be measured

with the final setup.

4.4 Pressure imbalance measurements

A pressure imbalance test was done to find the slope of the fit on the pressure imbalance δ values. Due to the fact that the zero enrichment correction only will affect the intersection parameter of the fit, the zero enrichment effect was not included in the pressure imbalance slope calculation. All measured δ values can be seen in figure 3.4. The sample inlet flow was changed with the back pressure regulator when measuring the δ values. For the duplicate measurements on the same pressure levels the δ where not identical, and it was found that δ values on the same pressure level diverged more, when the intensity difference between sample and reference was larger. The pressure regulators were tricky to operate and I suspect that the divergence is a mechanical effect in the pressure regulator valve, causing a slight change in intensities due to the pressure being slightly different.

From figure 3.4 measurement from different days have been used, the manual scan (yellow squares) was made on an earlier time where the line were still being modified. When calculating the slopes it was done with data from the acquisition runs. The reference intensity on mass 28 was $2V$ on the manual scan, and $1.9V$ on the isodat acquisition. The reference intensity on mass 40 was $1.6V$ on the manual scan, and $1.5V$ on the isodat acquisition.

From $\delta^{15}N$ it can be seen that the slope is steeper when the sample intensity is approximately $4V$ or below for both the manual scan and the acquisition. For $\delta^{40}Ar$ measurements from the acquisition the slope is first positive when the signal intensity on mass 40 is below approximately $4V$, but negative on the rest of the data. The same is not seen on the manual scan, why that is unclear. Therefor when working with the acquisition it should be made sure the intensities of mass 28 and 40 is above 4 volts.

With the setup I used this was the case with pressure set points above $40mbar$. Since the intensities for the final setup would be larger than $4V$ on mass 28 and 40, and to compare my values with those of Jesper Baldtzer Liisberg, the data were removed where this was not the case. What was left is the δ measurements and can be seen in figure 3.5, 3.6 and 3.7. I calculated the $\delta^{40}Ar$ from the inverse of δ^{36} and $\delta\frac{40}{28}$ manually with the raw mass intensities from the acquisition, because Isodat Acquisition was not setup up to measure $\delta^{40}Ar$ and $\delta\frac{Ar}{N_2}$ directly.

I found the slopes to be $\alpha_{15N} = 5.517 \cdot 10^{-5} \frac{\permille}{mV}$, $\alpha_{40Ar} = 0.4161 \cdot 10^{-3} \frac{\permille}{mV}$ and $\alpha_{\frac{Ar}{N_2}} = 0.3584 \cdot 10^{-3} \frac{\permille}{mV}$. The R^2 of the fits where found with $R^2 > 0.99$ indicating high linearity. The signal intensities for the pressure imbalance tests had a large range of approximately $40V$, this range is much higher than for measurement campaign where the offset between sample and reference is in the order of $1V$. With a signal intensity difference much larger than one from a real measurement the δ values behaves linearly as expected (when the small flow data has been removed), but it has to be investigated in additional experiments if the slope for the large range of intensity difference is also valid for smaller intensities.

The slopes of the pressure imbalance measurements are in the same order of magnitude as of those found by Jesper Baldtzer Liisberg [17].

For a measurement campaign the pressure imbalance should be done weekly, and the suggestion to include a three point valve is necessary in order to measure the pressure imbalance slope in combination with the final setup.

4.5 Chemical slope measurements

The chemical slopes of $\delta^{15}N$ and $\delta^{40}Ar$ were successfully found to be $\alpha_{CS} = 7.176 \cdot 10^{-6}$ and $\alpha_{CS} = 0.07579$ respectively. It can be seen that $\delta^{40}Ar$ is more sensitive to changes in the gas composition by order of magnitude of 10^4 relative to $\delta^{15}N$, this may be contributed to the much lower concentration of argon compared to nitrogen in atmospheric air.

The uncertainties on $\delta^{15}N$ and $\delta^{40}Ar$ was found by the standard error from Isodat Acquisiton. The slope from $\delta^{15}N$ is in the same order of magnitude as Jesper Baldtzer Liisberg. For $\delta^{40}Ar$ I cannot compare since he did a second order polynomial regression on $\delta^{36}Ar$. The fits are within the bounds of the uncertainties but the R^2 values were not that great because we still see a non linear behavior.

4.5.1 Examining mass 36 from oxygen and argon

From figure 3.11 it can be seen that the $\delta^{40}Ar$ value changed approximately 60 ‰with a change in the mass 32 intensity of approximately $40V$. I suspected $^{18}O^{18}O$ is the cause of relatively large deviation in the δ value.

The abundance of $^{18}O^{18}O$ in the atmosphere is found by multiplying the isotopic abundances of two ^{18}O atoms forming a $^{18}O^{18}O$ molecule with the concentration of O_2 in air, the abundance of the isotopes can be read from table 2.1 and the atmospheric concentration of oxygen can be read from table 2.2. The calculation becomes $^{18}O^{18}O = 0.00205^2 \cdot 0.2095$. The same can be done for the isotope of argon with mass 36, $^{36}Ar = 0.0033 \cdot 0.0093$. The ratio between these two gives an approximate value of the change in the δ. The gas composition changes when the volume of oxygen was released and the measured signal on mass 28 dropped by approximately 60%. A rough calculation based on the assumption that the removed nitrogen is replaced by oxygen, finds that the gas now consist of 58% oxygen. The expected change in the δ value due to $^{18}O^{18}O$ molecule being measured on the same cup as ^{36}Ar and assuming constant argon concentration, is expected to be: $\frac{0.0025^2 \cdot 0.58}{0.0033 \cdot 0.0093} \cdot 1000‰ = 79.42‰$. This is within the same order of magnitude as the change observed from the measured $\delta^{40}Ar$ and explains the large change in $\delta^{40}Ar$.

4.5.2 Adding oxygen and carbon dioxide

A note to reading the chemical slope measurements where oxygen(figure 3.10,3.11 and3.12) and carbon dioxide (figure 3.13, 3.14 and 3.15) was added when following the time per-

spective. First a reference level was measured, this is where the δ values were zero. Then the valve on the volume containing pure oxygen or carbon dioxide was opened. The largest δ values where found after this, while the volume emptied over time the δ values became smaller.

For figure 3.10 and 3.12 the δ value never reaches the reference level again. This effect is not quite understood but could be due the absorption processes of oxygen in the capillary, also the oxygen could react with nitrogen in the ions source and form NOx which could alter $\delta^{15}N$. We don't see this effect on figure 3.11 which adds to the explanation because $\delta^{40}Ar$ is not effected in that from NOx formation.

For figure 3.13 the chemical slope between $\delta^{15}N$ and carbon dioxide looks quite linear, there is however a fast drop in $\delta^{15}N$ and $\delta\frac{Ar}{N_2}$ at $2200mV$ on mass 44, this could be due to CO(m28) being created in the mass spectrometer, from fragmentation of CO_2. CO would be measured on mass 28, so an increase in the carbon dioxide would increase the chance of the CO molecule of being formed, thus decreasing the $\delta^{15}N$ and $\delta\frac{Ar}{N_2}$. The same effect can be seen in figure 3.15 for mass 44 intensities larger than $7V$. Between $3.5-6V$ of mass 44 the increase in $\delta\frac{Ar}{N_2}$ can be explained by NOx being formed, decreasing the N_2 with mass 28, thus increasing the δ value. The two effects would alter the δ values in opposite direction. Also a change in the ionization efficiency with changing gas composition could partly explain results shown in figure 3.10 and 3.15.

From figure 3.14 the $\delta^{40}Ar$ value was changed less than 1 ‰.

For figure 3.15 the δ behaves quite non-linear. A repetition of the chemical slope measurements for oxygen and argon could be made, to the amount of time required for the δ to revert back to the reference level and to fill the data gap on the intensity range of 1.3 to 2.0 V on mass 44. This would provide additional information into how long it takes for the specific setup to be usable after any of the lines have been exposed to the laboratory air.

Due to the stickiness of oxygen and carbon dioxide it took $+3$ hours for the intensity and δ values to revert back to levels before the gases where introduced. This was only with a very small gas volume only added to the last capillary before entering the mass spectrometer. When the line was opened when something needed to be changed, and the larger metal tubes were exposed, it took more than a day for the mass intensity levels of oxygen and carbon dioxide to revert back from atmospheric levels.

To prevent reactions inside the source or the line that will tamper with $\delta^{15}N$ and $\delta^{40}Ar$ it is necessary to remove as much as possible of carbon dioxide and oxygen. It was found that introducing oxygen influenced the δ values more than nitrogen, argon and carbon dioxide.

4.6 Carbon dioxide removal

The scan in figure 3.16 shows both the effect on the mass intensities by heating the oven and adding liquid nitrogen to the dewar. Arrows has been added to the plot to showcase this. Unfortunately not all carbon dioxide was removed. The ratio of carbon dioxide

remaining in the gas was found to be $\frac{1948.3}{12805}mV = 0.15$. The atmospheric level of carbon dioxide at the time when the NEEM air was sampled was at $393.12ppm$. This means that $57.82ppm$ where left in the sample gas. This level of removal of carbon dioxide was deemed sufficient based on the fact that the carbon dioxide chemical slopes for $\delta^{15}N$ and $\delta^{40}Ar$ were relatively small compared the chemical slopes from adding nitrogen, oxygen and argon. To further reduce the carbon dioxide removal a longer steel tube could be submerged in the dewar or a second trap could be installed in the line.

4.7 Oxygen removal measurements

The oxygen removal rates were found and can be seen in figure 3.18 and 3.19. From the temperature test it can be seen that it takes more than approximately 4000 seconds for the removal rate to go into equilibrium when a change in the temperature was made, this was a general issue that caused testing to take a very long time. From the temperature testing it is also seen that the oxygen removal does not work better at higher temperatures, the highest removal rate was found at $658.8°C$. This conflicts with previous findings [17][34]. They found the optimal working set point to be $950°C$. It was not possible to reach this temperature with the used power supply. However the removal rates are higher than 99.2% for the whole investigated temperature range ($658.8 - 790.0°C$) and thus considered as efficient enough for the $\delta^{15}N$ and especially for the $\delta^{40}Ar$ measurements. With a removal rate of 99.2% I would expect the change on $\delta^{40}Ar$ to be $0.28\%_0$ due to $^{18}O^{18}O$.

From the test with a constant temperature and changing helium flow as seen in figure 3.19, it can be concluded that helium is the most important factor in the oxygen removal process. Approximately $80\frac{ml}{min}$ was the highest helium stream I could achieve with the flow regulators that were available. The helium stream removal efficiency depends on the size of the inner diameter of the reactor quartz tube. A change to a smaller diameter would increase the removal efficiency. It should be noted that the flow meter measuring the helium flow into the oven drifted approximately $2\frac{ml}{min}$ per day. Zeroing it should be done on a daily basis.

In my experiments a change was made to a $\frac{1}{4}$" quartz tube instead of a $\frac{5}{8}$", unfortunately it was discovered that the membrane piece had been broken when measuring data for the oxygen removal efficiency of the smaller quartz tube. Jesper Baldtzer Liisberg found a removal rate of 98.5% [17], Bianca Xuan Nguyen Larsen found a removal rate of 99.9% [34], I found a removal rate of 99.4% at much lower temperature. A reason for the good removal rates at lower temperatures could be could be that the perovskite membranes has been lying on a shelf for several years and it is unknown if the performance was affected from the membrane being exposed to water vapor in room air. I did not examine if the oxygen removal rate from the membrane was dependent on the membrane length or if the membrane worked with the same efficiency over long periods of time. These parameters could be examined to test the performance difference between the membrane I used and ones of Jesper Baldtzer Liisberg and Bianca Xuan Nguyen Larsen.

4.8   Final measurements with oxygen removal

I examined the stability of the final setup by measuring four different acquisitions runs. The measured $\delta^{15}N$ and $\delta^{40}Ar$ was proven to be stable when the zero enrichment, pressure imbalance and chemical slope was corrected. The uncertainty on the delta value was found by propagating the different standard deviations of the measurement data and parameters used in the corrections. For both $\delta^{15}N$ and $\delta^{40}Ar$ The uncertainty on the first three acquisition run did not change by a significant digit, but for run 4 there the uncertainty were respectively 3 and 2 times bigger with the corrections due to the term including the intensity difference between reference and sample blew up.

For the final measurements a quartz tube of $\frac{1}{4}$" was setup and a Swagelok nut with a $\frac{1}{4}$" ferrule was installed. This was done because of the suspicion that the o-rings in the Ultra-Torr connections were releasing absorbed carbon dioxide and oxygen when heated. It could also be that the o-rings became slightly permeable to air due to expansion from heating. I had no way of measuring the temperature at the glass near the o-ring but the quartz tube were too hot to touch. To correct for this a longer quartz tube could be installed, this would however have the drawback of increasing the risk of the quartz tube breaking and complicates the installation of the membrane.

A test was conducted to test if a counter flowing helium stream produced better results, the oxygen removal efficiency was bad (in the order of 50%), unfortunately it was discovered that the membrane broke when setting up the stream, and the data was discarded. Therefor it was not tested if a higher level of oxygen removal could be achieved with a counter flowing helium stream.

Optimally an even smaller quartz tube with an inner diameter barely bigger then the outer diameter of the membrane could be installed. This would reduce amount of helium required to remove oxygen.

4.9   Complications in the oven building

Throughout the oven building process problems arose and here is a description of how they were dealt with.

The heating wire was initially coiled by mounting the quartz tube to a lathe. This proved difficult and a few quartz tubes where damaged due to stress on the end, the solution was to coil the wire by hand which made it more difficult to get the coil tight, but the result was the quartz tubing didn't break. Choosing the correct wire was difficult since I didn't know what power was required to reach the temperature of $950°C$ and several wires burned through due to the current in the wires being too high, this destroyed both the wire and the insulating cement. One major problem was having enough coils to produce the heating without burning the wire from the current. I tested with Omega nickel chromium resistance wire with 1.35 and $21.0\frac{\Omega}{m}$. The first didn't provide enough power with the amount of coils I could fit into the quartz tube and the second was broken several times due to the high current. For a long period the second option worked well at

approximately $950°C$, but after running for $+10$ hours the wire burned through. Finally the thermocoax wire was chosen, which also had the added benefit of being electrically insulated so no short circuit happened if the wire accidentally came in contact with the metal frame. The temperature control was also tested with a PID and might be smarter for future use, I however ended up changing the voltage directly at the power supply due to easier fine tuning of the temperature.

I also did testing with a transformer that could transform the outlet 220 AC into different predetermined set points between $40V$ and $80V$. However it was broken for voltages above $50V$ causing the laboratory fuse to go off. This transformer was rejected and the DC power supply was used instead.

One wire was broken due to turning off the PID and the temperature dropping approximately $200°C$ in a minute, so a gradual heating and cooling was implemented.

The membrane was very fragile several pieces were broken due to not being handled delicately enough. Initially the membrane was locked into place in the reactor tube by ceramic pieces, but the long working wire of 10+ hours, produced elevated temperature when it was destroyed, which caused the ceramics and gold paste to melt and the membrane to burn into it. This made the entire quartz tube piece unusable and brittle. The solution was to rest the membrane directly on the quartz tube, however one membrane broke from rotating the quartz tube 180° along the cylinder axis. Delicacy regarding handling the membrane and the quartz tube was a must.

4.10 Forward pressure regulator valve

The forward pressure regulator controller valve was broken, the percentage the valve was open it did not work in the range $0 - 23\%$. Even though the valve was reading 10%, no pressure change would happen until the valve was 23% open, causing a large overshoot. This caused the pressure to never stabilize but oscillate around the set point. To fix this the k-speed parameter of the valve had to be overwritten, k-speed as a factor applied to the other control parameters and essentially controls the response time of the valve. The k-speed was changed between 10-60, fabrication level is 1. Another artefact of this problem was that the set point should be changed more than $10mbar$ per stop, otherwise the pressure would oscillate and never become stable.

Chapter 5

Conclusion and outlook

Through the course of this thesis the measurement setup measuring $\delta^{15}N$ and $\delta^{40}Ar$ from gas extracted from ice core samples was successfully modified and rebuilt. This includes producing a new oven and preparing new perovskite membranes used for removing oxygen from the sample line.

The oxygen removal efficiency from the perovskite membrane was tested and found to be 99.4%, this includes both dependency on temperature and the helium stream. It was found that the helium flow rate in the reactor tube was the most important factor as long as the oven temperature was above the activation limit of the membrane.

To correct the final δ values a series of measurements were made. The zero enrichment corrections were determined to be $Z.E.M\delta^{15}N = 0.0464 \pm 0.0030$‰ and $Z.E.M\delta^{40}Ar = -0.1220 \pm 0.0450$‰.

The pressure imbalance slopes were determined to be $\alpha_{PI^{15}N} = 5.517 \cdot 10^{-5}\frac{‰}{mV}$, $\alpha_{PI^{40}Ar} = 0.4161 \cdot 10^{-3}\frac{‰}{mV}$ and $PI\alpha_{\frac{Ar}{N_2}} = 0.3584 \cdot 10^{-3}\frac{‰}{mV}$.

The chemical slopes were determined to be $\alpha_{CS\delta15N} = 7.176 \cdot 10^{-6}$ and $\alpha_{CS\delta40Ar} = 0.07579$.

The stability of the setup was tested with air sampled from the NEEM ice core location. Four different measurements were successfully performed where the $\delta^{15}N$ was found to be: 4.787±0.0120‰, 4.785±0.0060‰, 4.649±0.0070‰ and 4.503±0.0689‰. The $\delta^{40}Ar$ was found to be: 6.078±0.1581‰, 6.064±0.0991‰, 5.8465±0.0722‰ and 5.8519±0.3687‰.

5.1   Outlook

The final setup seen from figure 2.10 and 2.9 did not include the option to measure the zero enrichment, pressure imbalance slope and the chemical slope. Installing a three point valve on the mass spectrometer inlet line is necessary to resolve this issue. I suggest mounting a three point valve on the mass spectrometer casing. This can be connected the inlet valve capillary, the sample stream capillary and a capillary connected to a line with the gas that needs to be introduced.

Unfortunately I did not have time to test the setup in combination with the larger ice melting line of the CFA system. Creating bubble free ice and using the gas extraction

system would allow to test the system that was built, prior to a future measurement campaign. This would also allow to test the solubility effect which is the effect where a fraction of the gas gets dissolved in the melted ice.

To get the most efficient oxygen removal a smaller quartz tube could be installed. This would lower the amount of helium required to carry away the removed oxygen. The efficiency could also be tested with a helium stream flowing in the opposite direction of the sample stream.

Inserting the capillaries inside the membrane was extremely tricky and the membrane and capillaries broke several times. A solution could be fix the membrane in place inside the quartz tube, inserting the capillaries would be easier this way and it would make sure that membrane was always placed in the correct position in the hot part of the oven. A similar solution to what I tried to implement with ceramic pieces could be implemented, this however has the drawback of difficulty in removing the broken parts if the wire or the membrane breaks.

Understanding why the pressure imbalance had a positive slope from the low intensities and a negative on the larger intensities from the acquisition was never clear. A further investigation of this effect would help illuminate why this was the case.

Bibliography

[1] S. T. D. Q. G.-K. P. M. T. S. A. J. B. A. N. Y. X. V. Bex and P. Midgley, *Climate change 2013: the physical science basis. contribution of working group i to the fifth assessment report of the intergovernmental panel on climate change* (Cambridge University Press, 2013).

[2] P. Kindler, "Ngrip isotopic gas measurements from 10 to 38 kyr and a temperature reconstruction for the last glacial", PhD dissertation (Physikalisches Institut der Universität Bern, 2013).

[3] M. C. Leuenberger, C. Lang, and J. Schwander, "Delta ^{15}N measurements as a calibration tool for the paleothermometer and gas-ice age differences: A case study for the 8200 B.P. event on GRIP ice", jgr **104**, 22, 163–22, 170 (1999).

[4] A. Mariotti, "Atmospheric nitrogen is a reliable standard for natural 15n abundance measurements, nature", Nature **303**, 685–687 (1983).

[5] W. Dansgaard, S. J. Johnsen, J. Møller, and C. C. Langway, "One thousand centuries of climatic record from camp century on the greenland ice sheet", Science **166**, 377–381 (1969).

[6] C. Lang, M. Leuenberger, J. Schwander, and S. Johnsen, "Rapid temperature variation in central greenland 70,000 years ago", Science **286**, 934–937 (1999).

[7] W. G. Mook, *Environmental isotopes inthe hydrological cycle: principles and applications vol. 1*, 2nd ed. (2001).

[8] J. Hoefs, *Stable isotope geochemistry*, 6th ed. (Springer, 2009).

[9] T. Blunier and M. Leuenberger, *Stable isotopes* (2008).

[10] D. Kuroiwa, "Study of ice sintering", Tellus **13:2**, 252–259 (1961).

[11] B. C., "Studies of firn air", he Encyclopedia of Quaternary Science **2**, 361–372 (2013).

[12] K. Takuro, S. Jeff, and K. Kenji, "Argon and nitrogen isotopes of trapped air in the gisp2 ice core during the holocene epoch (0-11,500 b.p.): methodology and implications for gas loss processes", Geochimica et Cosmochimica Acta **72**, 4675–4686 (2008).

[13] J. S. B. Schwander, "Age difference between polar ice and the air trapped in its bubbles", Nature **311**, 45–47 (1984).

[14] M. M. HERRON and J. CHESTER C. LANGWAY, "Firn densification: an empirical model", Journal of Glaciology **25, No. 93**, P373–385 (1980).

[15] K. M. Cuffey and W. S. B. Paterson, *The physics of glaciers* (Elsevier, 2010), Chapter 2.

[16] T. Sowers, M. Bender, and D. Raynaud, "Elemental and isotopic composition of occluded o2 and n2 in polar ice", Journal of Geophysical Research: Atmospheres **94**, 5137–5150 (1989), eprint: `https://agupubs.onlinelibrary.wiley.com/doi/pdf/10.1029/JD094iD04p05137`.

[17] J. B. Liisberg, "Abrupt climate change and the nitrogen cycle", 2020.

[18] J. M. Wallace and P. V. Hobbs, *Atmospheric science an introductory survey*, 2nd ed. (Elsevier, 2006).

[19] S. J., "The transformation of snow to ice and the occlusion of gases", The Environmental Record in Glaciers and Ice Sheets, 53–67 (1989).

[20] Craig, H, Horibe, Y, Sowers, and Todd, "Gravitational separation of gases and isotopes in polar ice caps", Science (New York, N.Y.) **242**, 1675–1678 (1988).

[21] J. P. SEVERINGHAUS, A. L. GRACHEV, B. LUZ, and N. CAILLON, "A method for precise measurement of argon 40/36 and krypton/argon ratios in trapped air in polar ice with applications to past firn thickness and abrupt climate change in greenland and at siple dome antarctica", Geochimica et Cosmochimica Acta **67**, 325–343 (2001).

[22] A. M. Grachev and J. P. Severinghaus, "Determining the thermal diffusion factor for 40ar/36ar in air to aid paleoreconstruction of abrupt climate change", The Journal of Physical Chemistry A **107**, 4636–4642 (2003).

[23] A. Grachev and J. Severinghaus, "Laboratory determination of thermal diffusion constants for 29n2/28n2 in air at temperatures from -60 to 0°c for reconstruction of magnitudes of abrupt climate changes using the ice core fossil-air plaeothermometer", Geochimica et Cosmochimica Acta **67**, `10.1016/S0016-7037(02)01115-8` (2003).

[24] T. E. Corporation, *Mass spectrometry learning center*, `https://www.thermofisher.com/dk/en/home/industrial/mass-spectrometry/mass-spectrometry-learning-center.html`, Accessed: 2021-11-15.

[25] J. T. Watson and O. D. Sparkman, *Introduction to mass spectrometry : instrumentation, applications and strategies for data interpretation*, 4th ed. (John Wiley and Sons, 2008).

[26] T. Blunier, *Ion statistics note*.

[27] B. Lautrup, *Physics of continuous matter exotic and everyday phenomena in the macroscopic world*, Second edition (CRC Press, 2011).

[28] T. E. Corporation, *Isodat 2.0 operating manual*, 2004.

[29] N. P. Levitt, "Sample matrix effects on measured carbon and oxygen isotope ratios during continuous-flow isotope-ratio mass spectrometry", Rapid communications in mass spectrometry **28**, 2259–2274 (2014).

[30] T. E. Corporation, *Delta v plus operating manual*, 2005.

[31] J. F. Carter and V. J. B. (eds), *Good practice guide for isotope ratio mass spectrometry*, 2011.

[32] M. L. Bender, P. P. Tans, J. Ellis, J. Orchardo, and K. Habfast, "A high precision isotope ratio mass spectrometry method for measuring the o2n2 ratio of air", Geochimica et Cosmochimica Acta **58**, 4751–4758 (1994).

[33] R. J. Barlow, *Statistics : a guide to the use of statistical methods in the physical sciences*, 4th ed. (Wiley, 2013).

[34] B. X. N. Larsen, "Oxygen removal from air of atmospheric composition", 2018.

[35] V. Z. S.P.S. Badwal F.T. Ciacchi and K. Giampietro, "Oxygen removal and level control with zirconia - yttria membrane cells", (2003).